Motion Control of Open Containers with Slosh Constraints

Grundelius, Mattias

1998

Document Version:
Publisher's PDF, also known as Version of record

Motion Control of Open Containers with Slosh Constraints

Mattias Grundelius

Department of Automatic Control
Lund Institute of Technology
Lund, Sweden

Department of Automatic Control
Lund Institute of Technology
Box 118
S-221 00 Lund Sweden

Document name
LICENTIATE THESIS

Date of issue
November 1998

Document Number
ISRN LUTFD2/TFRT--3222--SE

Author(s)
Mattias Grundelius

Supervisor
Bo Bernhardsson and Karl Johan Åström

Sponsoring organisation
Swedish National Board for Industrial and Technical Development (NUTEK) and Tetra Pak Research & Development AB

Title and subtitle
Motion Control of Open Containers with Slosh Constraints

Abstract

This thesis considers liquid motion within moving open containers. The objective is to determine the open-loop acceleration profile for moving the container in minimum time without excessive slosh. This very common problem in the packaging industry has a significant influence on production capacity and quality.

Traditionally, motion control problems have been solved with purely mechanical devices. The introduction of modern servo systems to control movement has increased flexibility and it is now possible to vary the acceleration profile depending on the product. Since the fluid dynamics of different products are very different (for example compare skim milk with yoghurt) they do not have the same optimal acceleration profile. This has lead to an increased interest in systematic methods for calculation of acceleration profiles.

Experiments show that slosh exhibits two nonlinear behaviors: amplitude dependent oscillation frequency and asymmetric oscillation. The surface elevation was measured with a infrared laser displacement sensor. A linear second order oscillator was used, which captures the basic behavior, to model the slosh. The acceleration profiles were calculated by solving different optimal control problems both numerically and analytically. The performance of the obtained acceleration strategies were evaluated in experiments.

The experiments show that the acceleration profiles calculated by solving a minimum-energy problem gives the best performance. The minimum-time strategies fails due to low model accuracy.

Key words
Motion Control, Optimal Control, Slosh Modeling, Slosh Measurements

Classification system and/or index terms (if any)

Supplementary bibliographical information

ISSN and key title
0280–5316

ISBN

Language
English

Number of pages
83

Recipient's notes

Security classification

Motion Control of Open Containers with Slosh Constraints

Motion Control of Open Containers with Slosh Constraints

Mattias Grundelius

Department of Automatic Control
Lund Institute of Technology
Lund, November 1998

To Andrea and Freja

Department of Automatic Control
Lund Institute of Technology
Box 118
S-221 00 LUND
Sweden

ISSN 0280–5316
ISRN LUTFD2/TFRT--3222--SE

Printed in Sweden by Reprocentralen, Lunds Universitet.
Lund 1999

Contents

Acknowledgments

I would like to thank colleagues, family, and friends for all the help and support I have received during this work. In particular, I would like to thank my supervisor Bo Bernhardsson for his comments, suggestions, and for always having time and Rolf Braun for his help with the measurement equipment. I also would like to tank Bo Hellberg, Robert Massey, Silviu Matei, Anders Sundberg, and Istvan Ulvros at Tetra Pak for their insight into the practical problems and their comments and my work.

This work has been supported by the Swedish National Board for Industrial and Technical Development under contract P6987-2. The experimental equipment has been supplied by Tetra Pak Research & Development AB, Lund. Which is greatfully acknowledged.

1

Introduction

This thesis deals with control problems in machines for packaging fluids. Such machines have traditionally been made as pure mechanical devices. With the advances in computers and electronics it is now possible to make cheaper and more efficient machines by using active control.

The problem of moving a package from one position to another is a key operation in the machines. It is essential that such operations can be performed fast and in a well controlled manner. This problem has traditionally been solved with ad hoc methods. A suitable acceleration profile is developed and a motion control system is then used to implement the desired motion.

Improved movement methods are directly reflected in production rate. Hence, it is easy to directly see the benefits of control. Liquid sloshing is a key factor in the movement problem because it is necessary to perform the motion so that the liquid does not splash out of the package or contaminates the glue needed for sealing the package.

Motion induced sloshing is a classical problem in control. It was first encountered in control of guided missiles in the aerospace industry. In this application it was found that fuel sloshing could result in instabilities. Similar problems have also been encountered in control of airplanes, see Graham and Rodriguez (1952), Crawley *et al.* (1989) and Bryson (1994).

Liquid sloshing is also a severe problem in transportation ships, see Armenio (1992).

Sloshing is also a difficult problem for trucks that transport liquid,

see Sankar *et al.* (1992).

Motion of liquid in large storage tanks during earthquakes have also created serious difficulties, see Venugopal and Bernstein (1996).

Lately movement of open containers containing liquid, e.g. molten steel and various beverages, has been investigated where the main goal is to move as fast as possible, see Feddema *et al.* (1997) and Dietze and Schmidt (1997).

More details about the problem are given in this introductory chapter which is organized as follows. In Section 1.1 the operation of a packaging machine is described. Section 1.2 presents the problem considered in this thesis. The motivation for studying this problem is given in Section 1.3. Section 1.4 presents the contributions of this thesis. An outline of the thesis is given in Section 1.5

1.1 The packaging machine

The operation of a packaging machine can be divided into three independent sub tasks: folding, filling and sealing. These tasks are performed simultaneously on three different packages. A schematic picture of a packaging machine is shown in Figure 1.1.

The folded package is placed in a holder that carries the package through the machine. The movement of the package is performed stepwise, the number of steps between the different sub tasks depend on the machine type. The same movement is applied in every step on all packages. The time it takes to produce a package is determined by the filling time, which is the slowest of the sub tasks, and the time it takes to move the package one step.

The package contains liquid when it is moved between the filling and the sealing stations. This motion induces liquid motion in the package. This is what we refer to as slosh. The amount of slosh depends on how the package is accelerated and the properties of the liquid. There are large differences between skim milk and yoghurt.

If there is too much slosh the liquid might splash on the surfaces that should be glued. This can result in packages that are not properly sealed and possibly not airtight. If the package is not airtight the storage time is decreased considerably. This is particularly critical for aseptic packages that are supposed to have a very long storage time.

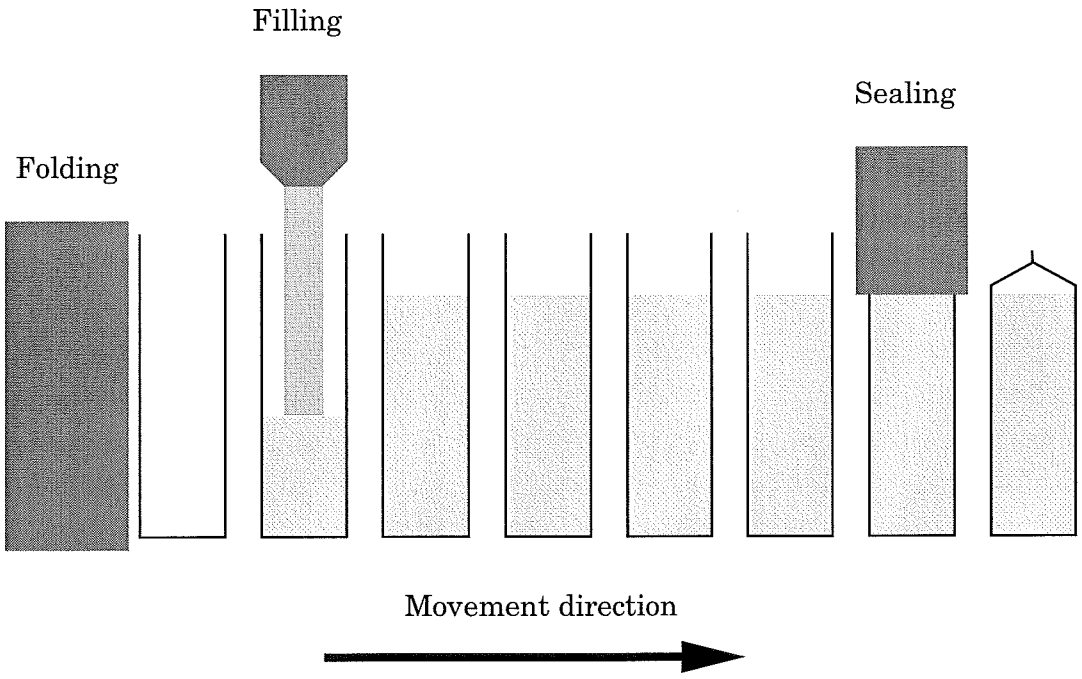

Figure 1.1 Schematic picture of the packaging machine.

The only way to increase the production capacity of the machine is by decreasing either the filling time or the movement time or both. This thesis considers the problem of decreasing the movement time. Liquid sloshing is the major constraint on the motion.

The movement of the packages is controlled by a servo system which control the position of the packages. A block diagram of the motion control system is shown in Figure 1.2. The reference is specified as an acceleration profile which is integrated twice to generate a position reference. The only measurements that are available to the servo system are the position and velocity of the package. Therefore, the only way to control the slosh is via open-loop acceleration control. This requires a very good model of the slosh.

The machine construction is very stiff so the liquid motion does not affect the motion of the package. The servo system is very fast so the actual acceleration of the package is very close to the specified acceleration reference. Therefore, the design of the position control and acceleration reference can be separated.

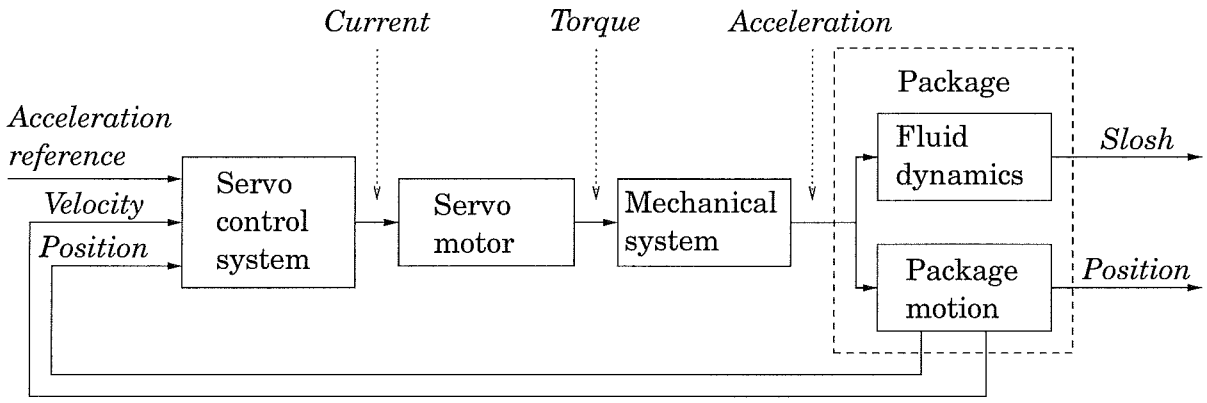

Figure 1.2 Block diagram of the motion control system.

1.2 Problem formulation

The problem is to derive a method for calculation of an open-loop acceleration profile that moves the package one step on minimum time with acceptable slosh. During the movement the slosh has to be bounded below a certain level. The problem can be divided into two cases: movement in several steps and movement in one step.

When the package is moved several times the same acceleration profile is applied at each step. Therefore, the acceleration must be such that the slosh constraint is not violated when the acceleration profile is repeated. One way to achieve this is to ensure that the slosh is in the same state at the beginning of each movement step. The natural choice of initial state of the slosh is that the liquid is at rest, since this is the state after the package has been filled.

When the package is moved only one step, we can allow some slosh after the movement has been performed, since the next time the package is moved it is sealed and we do not need to take the slosh into account.

1.3 Motivation

The main motivation for our work is that faster movement gives higher production capacity, and hence decreases the production cost of one package. This will give the packaging machine manufacturer an ad-

vantage in the competition. It is also of interest to understand the fundamental limitations. This may influence the design of future systems.

If the sloshing in the package can be decreased, the empty space above the liquid in the package can also be decreased, and hence the amount of packaging material needed in the package is decreased. This results in lower cost and also environmental advantages, since a package with less material produces less waste and consumes less natural resources when produced.

A systematic method for calculating acceleration profiles also simplifies the development process and decreases the development time. This results in lower development costs for the packaging machine manufacturer. It also makes switches between different products easier so that the same machine can be used optimally for different products.

1.4 Contribution

The problem is solved by deriving a mathematical model of the slosh phenomena. Optimal control techniques are then applied to calculate optimal acceleration profiles.

The slosh is investigated by experiments that show that it exhibits two nonlinear behaviors: amplitude dependent oscillation frequency and asymmetric oscillation. Several methods to measure the slosh are presented and evaluated. A simple model suitable for solving the optimal control problem is presented. The model used is a second order linear oscillator which captures the main behavior of the slosh phenomenon.

The acceleration profiles are calculated by solving different optimal control problems, both numerically and analytically. Experimental evaluation of the acceleration profiles show that the minimum-time strategy is so sensitive that it only works for small oscillation amplitudes, which result in a long movement time. The reason for this is that a large amount of energy are pumped in and out of the system and that the model does not describe the slosh with sufficient accuracy. By imposing additional constraints to limit the maximum energy in the slosh, it is possible to obtain acceleration profiles that work for slightly larger slosh amplitudes. However, the slosh amplitude when

this strategy works is still much smaller than the maximum allowed slosh amplitude.

As an alternative approach the acceleration profiles are then calculated by solving a minimum-energy problem with a fixed movement time. The movement time is chosen to be 10 to 20 percent longer than the calculated minimum movement time from the solution of the minimum-time problem. This strategy works well in the experiments and gives shorter movement times than those that are practically possible to achieve with the minimum-time strategy.

1.5 Outline of the thesis

The outline of the thesis is as follows:

Chapter 2 presents the experimental setup and the measurement equipment. The mechanical construction and the servo system are described. The slosh measurement problem is also presented and several measurement methods are described.

Chapter 3 presents the slosh modeling problem. A review of the slosh modeling problem is given. Experiments are presented that show some of the phenomena encountered in the slosh. The model of the slosh that is used when calculating the acceleration profiles is presented.

Chapter 4 presents several different methods for calculating acceleration profiles. The performance of the different acceleration profiles are also evaluated with experiments.

Chapter 5 presents the conclusions and future work.

2

Experimental setup

This chapter describes the experimental setup. Section 2.1 gives a description of the mechanical construction. The servo control system and the servo motor is described in Section 2.2. The slosh measurement problem is discussed in Section 2.3 and several different measurement methods are presented.

2.1 The mechanical construction

An experimental setup has been constructed by Tetra Pak Research & Development AB. The measurement devices have been developed and tested in collaboration with Tetra Pak Research & Development AB.

The setup consists of a carriage mounted on a belt driven by a standard servo system, see Figure 2.1 and Figure 2.2. The coupling between the motor and the belt determines the gear ratio; one revolution of the motor axis moves the carriage 0.05 m. The container and a slosh sensor are mounted on the carriage. At each end of the belt a mechanical switch is positioned that triggers the safety system when the carriage move over them. This ensures that the mechanical construction does not take any damage if the carriage runs into one end of the belt.

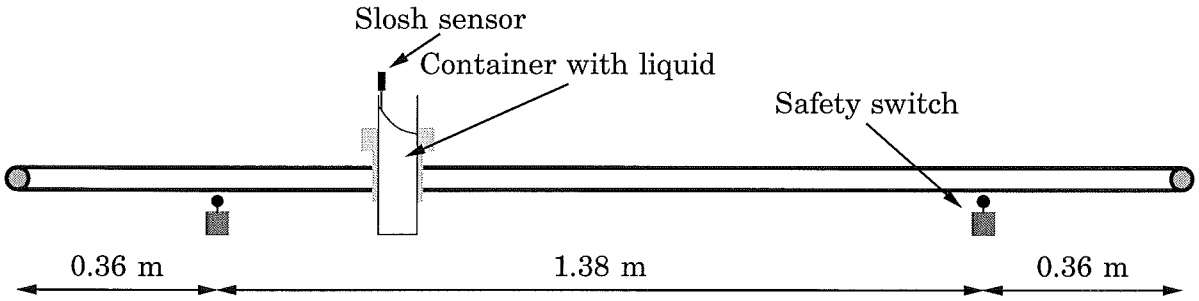

Figure 2.1 Schematic picture of the experimental setup.

2.2 The servo system

The control system is an Atlas DMC (Digital Motion Controller) model DMC50720P manufactured by Atlas Copco, see Figure 2.2 for a picture of the system.

Control is performed by a PID controller and feedforward to compensate for inertia (acceleration), viscous friction (velocity) and static friction (sign of the velocity). The control loop is sampled with a period time of 1 ms. The acceleration profile is given either as a acceleration reference stored in the memory or as a velocity reference read from the analog input at a sample rate of 5 ms. The acceleration reference is specified as a list of (acceleration-duration) pairs, where the acceleration is given in resolver increments and the duration in milliseconds, both as integers.

When the acceleration profile is specified as an acceleration reference the whole range of the available types of feedforward is utilized and the feedback loop is a PID-controller controlling the position with a position reference generated from the acceleration reference. When the acceleration profile is given as an externally generated velocity reference no feedforward is used and the feedback loop is a P-controller controlling the velocity.

All experiments are performed with the acceleration profile stored in the memory. Since this gives the best control performance due to the feedforward.

The servo motor is a four pole synchronous permanent magnetized AC motor manufactured by ELMO. The control system feeds the servo motor via a frequency converter with a switching frequency of 4 kHz.

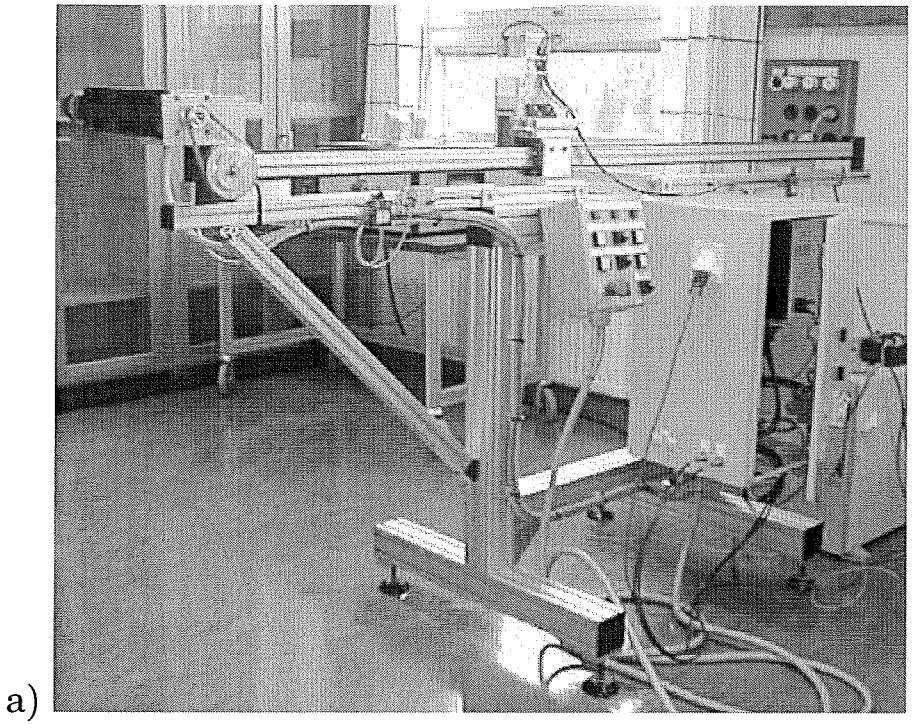

a)

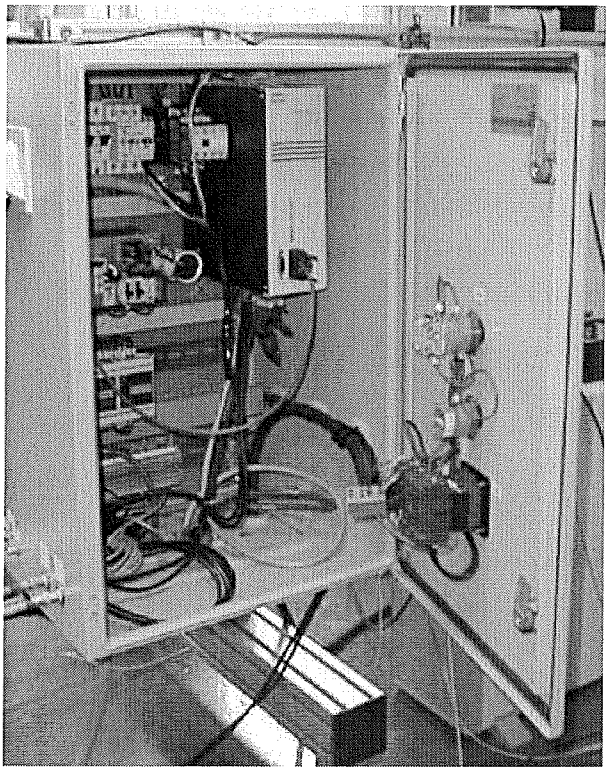

b)

c)

Figure 2.2 Photographs of the experimental setup. (a) Overview of the experimental setup, (b) close-up on the cabinet with the DMC and power supply and (c) close-up on the container and the laser displacement sensor.

2.3 Slosh measurements

The slosh measurement is needed for modeling of the slosh phenomena and for performance evaluation of the designed acceleration profiles. Ultimately, one would like a measurement of the surface profile and the flow velocity within the liquid. This is, however not possible today.

The surface profile can be captured by filming the container. This has been done at Tetra Pak for performance evaluation of the acceleration profiles. No direct measurements of the surface elevation were previously performed by Tetra Pak.

The most important measure for our problem is the surface elevation at the walls of the container, since the largest oscillations appear there and the constraint is that the surface does not reach a certain level on the wall.

The measurement problem turned out to be nontrivial. A number of sensors were evaluated during a period of one year. The infrared laser sensor described last is used today.

Pressure based measurement

The first attempt to get a measure of the surface elevation was to measure the pressure below the surface. A setup with two aluminum pipes with a diameter of 6 mm where put at each side of the container as shown in Figure 2.3. The pipes where connected to the pressure sensors by plastic tubes.

This worked well when the surface was at rest, but when the sur-

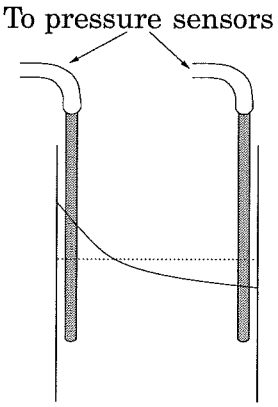

Figure 2.3 Illustration of the pressure measurement setup.

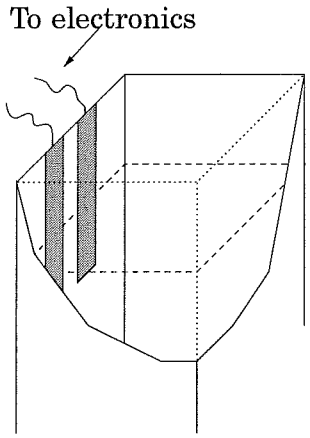

Figure 2.4 Illustration of the capacitance measurement setup.

face was moving the measurement did not reflect the actual surface elevation. This was due to the fact that when the liquid is moving the pressure does not only depend on the height of water above but also on the flow. This is a well known fact from hydrodynamics and now also known by us.

Capacitance based measurement

This method uses the difference in permittivity between water and air to measure the surface elevation. The capacitance between two conductors is dependent of the permittivity of the medium. The sensor is built up by two strips of 12 mm wide copper tape attached parallel to each other 5 mm apart on the outside of one of the walls of the container as shown in Figure 2.4. Depending on the water level on the inside of the wall the capacitance between the two copper strips changes.

This gives a good measure of the surface elevation when the surface is at rest, but when the surface is oscillating, a thin layer of liquid stays on the container wall. This thin layer of liquid destroys the measurement. The thin liquid layer moves down much slower then the surface oscillation, which results in a very slow decay in the measured surface elevation.

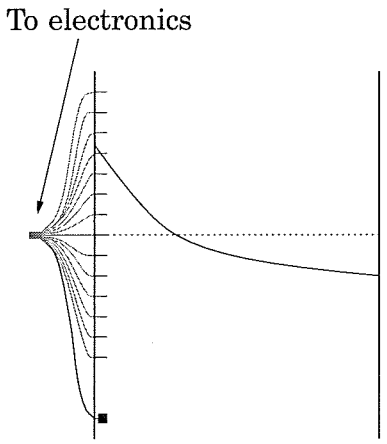

Figure 2.5 Illustration of the contact based measurement setup.

Ultrasonic based measurement

A standard ultrasonic distance sensor was also tried. It gave a good measure of the distance to the surface when the surface was at rest or moved slowly. But when the surface was moving to wildly the sensor lost track of the surface.

Electrical contact based measurement

In this method the electrical conductivity of water was used to measure the surface elevation. The sensor is built up by 14 pins, mounted 5 mm apart through the container wall, and one ground plate, see Figure 2.5. The measurement of the surface elevation is generated as a sum of all pins in contact with the ground plate. This gives an output that can take 15 different values.

The main drawback with this method was the low accuracy when measuring small oscillations. There were also some minor problems with drops of water sticking to the pins and the thin layer of water sticking to the container wall.

Infrared laser based measurement

A laser displacement sensor manufactured by Keyence Corporation, sensor head model LB-11(W) and controller model LB-70(W), has been used to measure the surface elevation.

The sensor is based on an infrared laser ray sent out from the sensor and detected by a photo detector. The ray is sent out with a certain

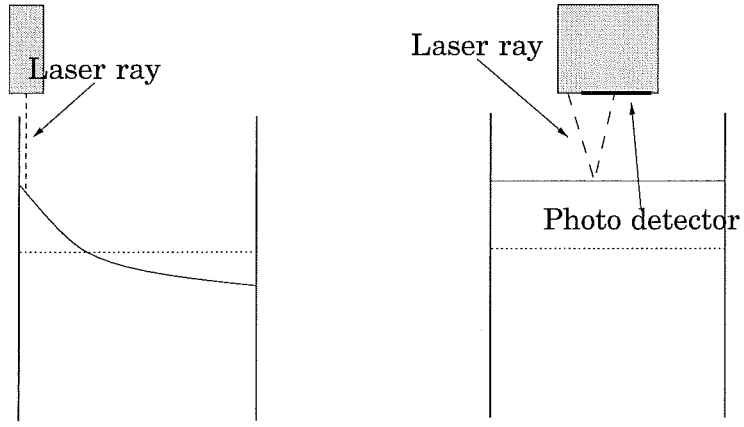

Figure 2.6 Illustration of the infrared laser based measurement setup. The left figure shows the container from the side and the right figure from the front

angle from the sensor and the point where the reflected ray hits the detector depends on the distance to the surface, see Figure 2.6.

The measurement range of the sensor is 60 mm to 140 mm. The response speed of the sensor can be set to 0.7 ms, 20 ms or 500 ms giving a 3 dB drop in the frequency response at 700 Hz, 18 Hz and 0.6 Hz respectively and a resolution of 180 μm, 40 μm and 10 μm . In the measurements the fastest response speed, 0.7 ms, was used. For water the reflection of the laser ray is poor, therefore the water was dyed with white paint in order to increase the reflection.

The sensor gives a good measure of the surface elevation and only occasionally loses track of the surface. The occasions when the sensor loses track of the surface are easily identified, since the output saturates at the lower limit when this happens. The sensor can be mounted both in the front and in the back of the container, see Figure 2.2.

Sensor calibration To investigate the linearity of the sensor, the sensor was calibrated by placing a flat white surface at a number of known distances from the sensor (the distance was measured with a mm graded ruler). The output of the sensor was sampled for one second with a sampling period of 5 ms at each distance. The mean value of each measurement series was then used to find the coefficients of the calibration transform

$$y = ax + b$$

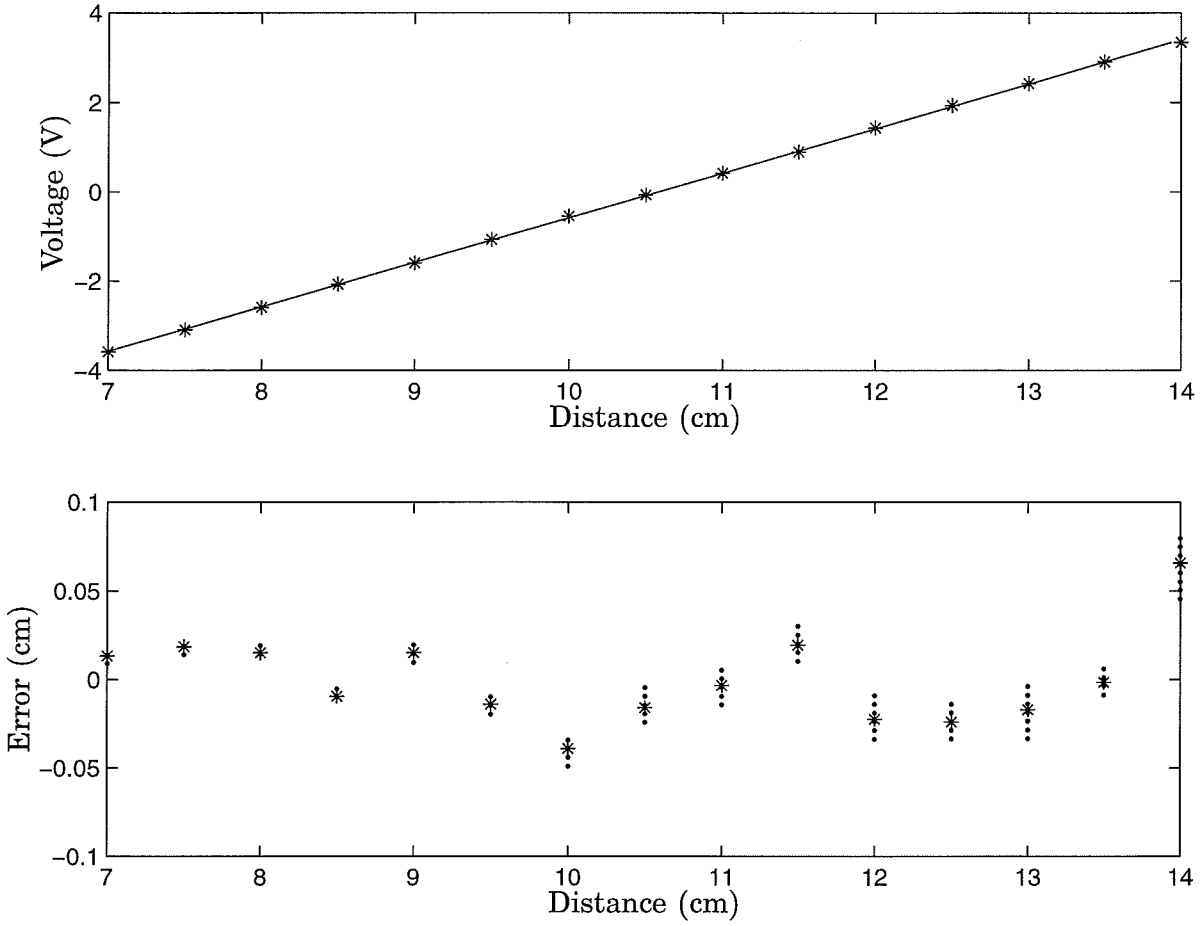

Figure 2.7 Data from the calibration; mean of each measurement series (∗) and the result when the calibration transform is used (upper), the error in distance when the calibration transform is used (lower) where (∗) is the mean error and (·) is the error for each point in the data series.

where y is the distance and x is the measurement. This resulted in the coefficients $a = 1.0036$ and $b = 10.5831$. The coefficients were calculated with the function `polyfit` in Matlab. Figure 2.7 shows the calibration data. In the figure it can be observed that the variance in the measurement is larger for the longer distances. Since the distance was measured by hand, the accuracy of the distance measurement is approximately ± 0.5 mm. The sensor calibration shows that the linearity of the sensor is good and that the resulting measurement error is probably less than 1 mm.

3

Slosh modeling

This chapter describes the slosh phenomenon. In Section 3.1 the equations governing the flow in a fluid is described. Section 3.2 presents some numerical and analytical solutions to the flow problem. An experimental investigation of the slosh phenomenon is presented in Section 3.3. In Section 3.4 the slosh model used in the optimization is presented.

3.1 Fluid dynamics

This section gives a description of different mathematical descriptions of fluid flow, for further details see Shen (1993), Baldock and Bridgeman (1981), Coulson (1955) and Lamb (1945).

Within the fluid

Fluid motion within the liquid is described by the so called *Navier-Stokes equations*. This is a set of nonlinear partial differential equations. The first equation describes the conservation of mass

$$\frac{\partial \rho}{\partial t} + \nabla \cdot (\rho \mathbf{v}) = 0 \tag{3.1}$$

where ρ is the density of the fluid and $\mathbf{v} = (u,\ v,\ w)$ is the velocity vector field. Equation (3.1) is referred to as the *continuity equation* in continuum mechanics.

The conservation of mass gives only one equation, but has four unknowns: $\mathbf{v} = (u, v, w)$ and ρ. Therefore, one needs some additional conditions, unless the density ρ is known and the problem is one dimensional. The extra condition is the conservation of momentum (i.e. Newton's Second Law of Motion). For a Newtonian viscous fluid the the conservation of momentum gives the equation

$$\rho\left(\frac{\partial \mathbf{v}}{\partial t} + (\mathbf{v}\cdot\nabla)\mathbf{v}\right) = -\nabla p + (\lambda+\mu)\nabla(\nabla\cdot\mathbf{v}) + \mu\nabla^2\mathbf{v} + \rho\mathbf{f} \tag{3.2}$$

where p is the pressure, λ the factor of volume compression, μ the viscosity and $\mathbf{f}$ the force vector field. Equation (3.1) and Equation (3.2) are called the *Navier-Stokes equations.*

If the fluid is incompressible ($\lambda = 0$) and inviscid ($\mu = 0$) the *Navier-Stokes equations* become the *Euler equations.*

$$\nabla\cdot\mathbf{v} = 0 \tag{3.3}$$

$$\frac{\partial \mathbf{v}}{\partial t} + (\mathbf{v}\cdot\nabla)\mathbf{v} = \frac{1}{\rho}\nabla p - \mathbf{f} \tag{3.4}$$

If the velocity field of the flow is irrotational, i.e. $\omega = \nabla\times\mathbf{v} = 0$ where ω is called the *vorticity*, the flow is called a *potential flow.* The *Euler equations* (3.3) and (3.4) can be written as

$$\frac{D}{Dt}\left(\frac{\omega}{\rho}\right) = \left(\frac{\omega}{\rho}\cdot\nabla\right)\mathbf{v} \tag{3.5}$$

This equation is called the *vorticity equation.* Equation (3.5) has a solution when $\omega = 0$. Thus an irrotational flow exist in a Euler equation sense. If the curl of the flow velocity field $\mathbf{v}$ is zero the there exists a potential ϕ such that

$$\mathbf{v} = \nabla\phi \tag{3.6}$$

Now the equations (3.3) and (3.5) may be considered as the governing equations since they are dependent on (3.3) and (3.4). Equation (3.5) is satisfied if $\omega = 0$. Hence the only equation which needs to be satisfied is (3.3) which now can be written as

$$\nabla\cdot\nabla\phi = \nabla^2\phi = 0 \tag{3.7}$$

This equation is known as *Laplace's equation.*

When the flow is irrotational and the external force field $\mathbf{f}$ has a potential, $\mathbf{f} = \nabla V$, Equation (3.4) can be written as

$$\frac{\partial \phi}{\partial t} + \frac{p}{\rho} + \frac{1}{2}|\nabla \phi|^2 + V = C(t) \tag{3.8}$$

where $C(t)$ is an arbitrary function of time. This equation is known as the *Bernoulli equation.*

Further simplifications can be done when the wavelength is much larger than the liquid depth. It is then assumed that the horizontal flow velocity is independent of the depth. This gives the *shallow water equations.*

Validity of assumptions The approximation that the fluid is incompressible is valid for most liquids but not for gas. The approximation that the viscosity is zero is however more questionable, for water it is valid but not for yoghurt. Irrotational flow is a solution to the *Euler equations* and therefore possible in a mathematical sense. However, any flow in the real world has a non zero viscosity and a non uniform density, which always cause rotation of fluid elements. But in many cases the vorticity is so weak that the flow can be considered approximately irrotational.

On the fluid boundary

The boundaries in our problem are the package walls and the free surface of the fluid.

On the package walls the boundary conditions are

$$\frac{\partial \phi}{\partial v} = 0 \tag{3.9}$$

where v is the direction orthogonal to the wall.

On the free surface $z = \eta(x, y, t)$, we have two boundary conditions. The first arises from the external forces acting on the surface and is a dynamical condition, for *Laplace equation* we can express this with the *Bernoulli equation.*

$$\frac{\partial \phi}{\partial t} + \frac{p}{\rho} + \frac{1}{2}|\nabla \phi|^2 + V(x, y, \eta(x, y, t), t) = 0 \tag{3.10}$$

The second condition states that a fluid particle originally on the free surface will remain on the the surface forever and is a kinematic condition.

$$\frac{\partial \eta}{\partial t} + \frac{\partial \phi}{\partial x}\frac{\partial \eta}{\partial x} + \frac{\partial \phi}{\partial y}\frac{\partial \eta}{\partial y} = \frac{\partial \phi}{\partial z} \tag{3.11}$$

Now the we can solve for the potential ϕ satisfying (3.7) within the fluid and (3.9), (3.10) and (3.11) on the fluid boundaries.

3.2 Related work

In Armenio and La Rocca (1996) the fluid is modeled in two dimensions by both the Reynolds Averaged Navier-Stokes Equations (RANSE) for an incompressible flow and the Shallow Water Equations (SWE). Both problems are solved numerically with different finite element methods. RANSE is solved using a method called SIMAC (Semi-Implicit Marker And Cell) which uses a fixed stretched grid. Each cell in the grid can either contain fluid or not. The numerical solutions are compared with experiments that show good correlation with the numerical solutions.

The problem of free surface flows in domains with moving boundaries are described in Kelkar and Patankar (1997). The method handles two-fluid flows where the two fluids can both be incompressible or one of the fluids can be compressible. Moving grids are utilized to accommodate the motion of the domain boundaries. The volume-of-fluid technique is used for tracking the free surface between the two fluids.

In Romero and Ingber (1995) the fluid flow is described as a potential flow using Laplace equation. The dynamic boundary condition on the free surface is the damping-modified Bernoulli equation. The damping in the Bernoulli equation is a simple way to include viscosity in the model. The problem is solved using a boundary element method. The boundary on the free surface is updated to track the motion of the surface.

The flow problem is solved analytically in Venugopal and Bernstein (1996). The flow is described by Laplace equation and the boundary conditions on the free surface is described by the Bernoulli equation. Separation of variables is used to find the horizontal and vertical

modes. The Bernoulli equation is then used to find the time dependency. In the derivation it is assumed that the surface elevation is small. The derivation shows that a horizontal acceleration only excite the odd numbered oscillation modes.

This gives the following model of the slosh

$$\begin{aligned} \dot{x}(t) &= Ax(t) + Bu(t) \\ y(t) &= Cx(t) + Du(t) \end{aligned} \tag{3.12}$$

with

$$\begin{aligned} A &= \text{diag}\left(\begin{bmatrix} 0 & 1 \\ -\omega_1^2 & 0 \end{bmatrix}, \begin{bmatrix} 0 & 1 \\ -\omega_3^2 & 0 \end{bmatrix}, \ldots, \begin{bmatrix} 0 & 1 \\ -\omega_n^2 & 0 \end{bmatrix}\right) \\ B &= -\frac{4\sqrt{2a^3}}{\pi^2}\,\text{stack}\left(\begin{bmatrix} 1 \\ 0 \end{bmatrix}, \begin{bmatrix} \frac{1}{9} \\ 0 \end{bmatrix}, \ldots, \begin{bmatrix} \frac{1}{n^2} \\ 0 \end{bmatrix}\right) \\ C &= \frac{1}{g}\sqrt{\frac{2}{a}}\,\text{augment}\left(\begin{bmatrix} 0 & \cos\frac{\pi x}{a} \end{bmatrix}, \begin{bmatrix} 0 & \cos\frac{3\pi x}{a} \end{bmatrix}, \ldots, \begin{bmatrix} 0 & \cos\frac{n\pi x}{a} \end{bmatrix}\right) \\ D &= \frac{1}{g}\left(\frac{a}{2} - x\right) - \frac{4a}{\pi^2 g}\sum_{i=1,\ i\ \text{odd}}^{n} \frac{1}{i^2}\cos\frac{i\pi x}{a} \\ w_i &= \sqrt{\frac{ig\pi}{a}\tanh\frac{ih\pi}{a}} \end{aligned} \tag{3.13}$$

where a is the width of the container, h is the liquid depth, x is the position where we measure the slosh, ω_i is the oscillation frequency of the ith mode and n is the number of modes. The function *diag* gives a block diagonal matrix, *stack* joins the vectors vertically and *augment* joins the vectors horizontally.

The step response for this model is shown in Figure 3.1 for different numbers of modes. The model has a direct connection from the acceleration to the surface elevation, this gives an instantaneous jump in the surface elevation in the beginning of the step. If we include all oscillatio modes the direct term goes to zero. The figure also shows that the higher order oscillation modes have little influence on the behavior.

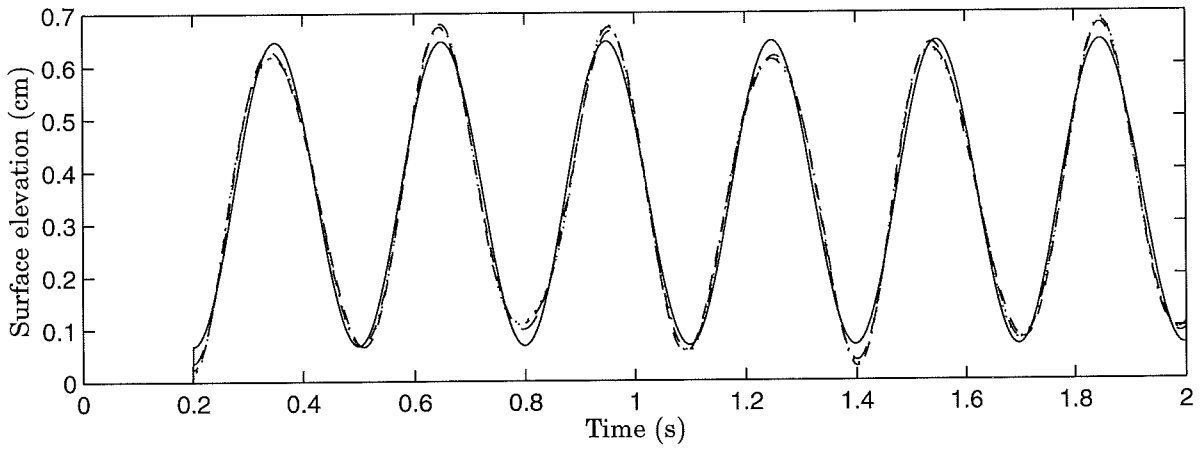

Figure 3.1 Step response for the model in Equation (3.12), with one mode (solid), three modes (dashed), five modes(dot-dashed] and seven modes (dotted).

3.3 The slosh phenomenon

The repeatability of the slosh phenomenon was investigated by running the same experiment several times. The acceleration profile given below was run five times, with $u_{max} = 3$ m/s^2.

$$u(t) = \begin{cases} u_{max} & 0 \leq t < 0.15 \\ -u_{max} & 0.15 \leq t < 0.30 \\ 0 & 0.30 \leq t \end{cases} \tag{3.14}$$

Figure 3.2 shows the results of the experiments. When the measurements from four different experiments are plotted on top of each other it is seen that the measurements are very close. The figure shows that even the measurement faults occur at almost the same time instants.

To get a measure of how close the experiments are the standard deviation is calculated for each time instant. The calculation of the standard deviation $\sigma(t)$ is given by

$$\sigma(t) = \sqrt{\frac{1}{4}\sum_{i=1}^{5}(s_i(t) - m(t))^2}\,, \qquad m(t) = \frac{1}{5}\sum_{i=1}^{5} s_i(t)$$

where $s_i(t)$ is the measured surface elevation of experiment i and $m(t)$ is the average of all experiments. The standard deviation $\sigma(t)$ is shown in Figure 3.3.

The figure shows that there are some very large peaks for $t < 0.5$, they are due to that the measurement faults do not occur at exactly the same time instants. In the right plot the time instants when the standard deviation is larger than 0.2 are removed (27 points were removed). This shows that the standard deviation is about 0.1 in the beginning (i.e. for large oscillation amplitudes) and about 0.01 in the end (i.e. for small oscillation amplitudes). The figure shows that the standard deviation is small compared to the measured value and the conclusion is that the repeatability of the slosh is very high.

To investigate the linearity of the slosh phenomenon the following acceleration profile is used for different values of u_{max}.

$$u(t) = \begin{cases} u_{max} & 0 \leq t < 0.4 \\ -u_{max} & 0.4 \leq t < 0.8 \\ 0 & 0.8 \leq t < 1.8 \\ -u_{max} & 1.8 \leq t < 2.2 \\ u_{max} & 2.2 \leq t < 2.6 \\ 0 & 2.6 \leq t < 3.6 \end{cases} \tag{3.15}$$

Figure 3.4 shows experiments with the acceleration profile in (3.15) for different values of u_{max}. If the slosh phenomena were linear, then the response normalized with u_{max} should be independent of u_{max}. Figure 3.5 shows the normalized surface elevation for some values of u_{max}, where the normalized surface elevation is defined as

$$s_N = \frac{\text{Surface elevation}}{u_{max}}$$

The figure shows that the normalized slosh is the same for $u_{max} < 1$, but for larger values the response is very different. Thus the slosh phenomena is nonlinear.

The slosh is an oscillation phenomenon,therefore a simple model would be a poorly damped second order linear system. The parameter-

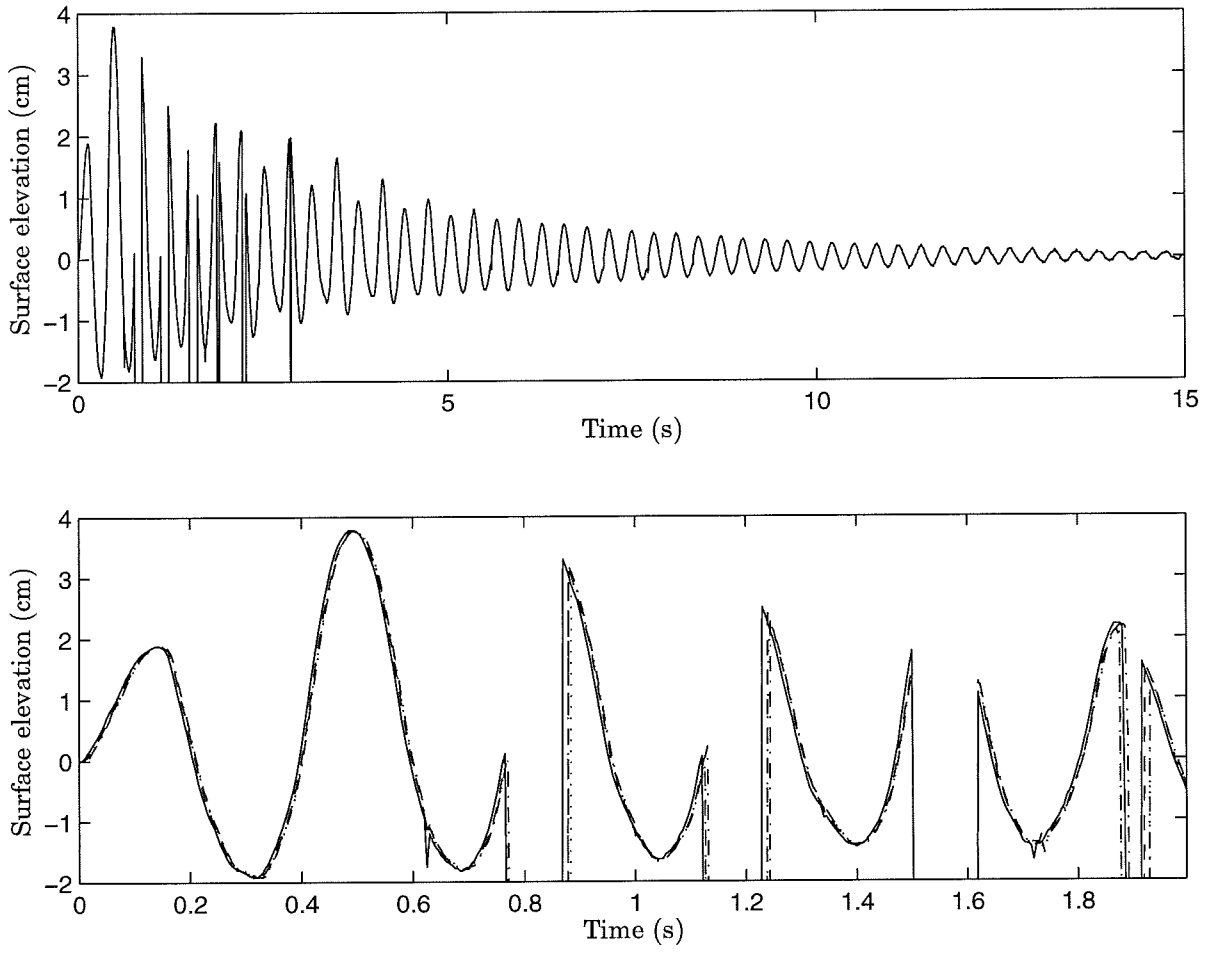

Figure 3.2 Results from experiments with the acceleration profile in (3.14) with $u_{max} = 3$ m/s^2. The upper plot shows measurements from one experiment, and the lower plot shows the measurements from four different experiments plotted on top of each other. The discontinuities at time 0.77 etc. are due to measurement faults.

ization of the transfer function is given below

$$G(s) = \frac{K\omega^2}{s^2 + 2\zeta\omega s + \omega^2} \tag{3.16}$$

The parameters of the transfer function in (3.16) was fitted using numerical optimization to the data from the experiments for different values of u_{max}. Simulations of the estimated models are shown in Figure 3.4 for different values of u_{max} and the estimated parameters are

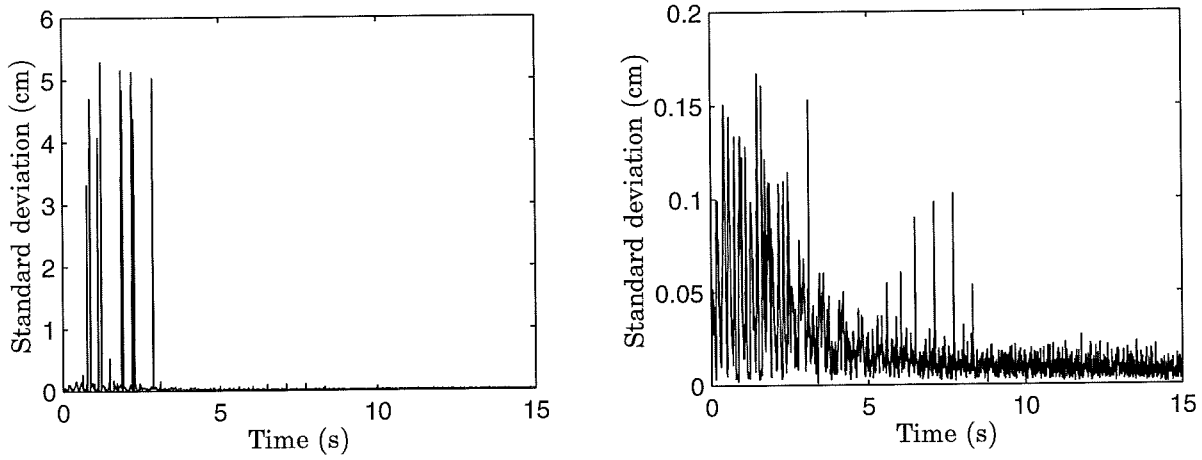

Figure 3.3 The standard deviation from the five experiments, the left plot shows the standard deviation for all values of t and in the right plot those instants when the standard deviation is greater than 0.2 are removed.

u_{max} (m/s^2)	K	ω (rad/s)	ζ
0.25	0.263	21.2	0.024
0.50	0.252	20.9	0.014
0.75	0.251	20.8	0.012
1.00	0.251	20.7	0.008
1.25	0.252	20.6	0.007
1.50	0.251	20.5	0.008
2.00	0.258	20.3	0.013
2.50	0.267	20.0	0.021
3.00	0.286	19.8	0.031

Table 3.1 Estimated parameters of the transfer function (3.16) for different values of u_{max}. The experiments indicates that ω is amplitude dependent.

shown in Table 3.1. The figure shows that the simulated surface elevation is very close to the measured surface elevation. In the table it can be observed that the estimated value of ω decreases with increased amplitude of the input u_{max}. This indicates that the oscillation frequency of the slosh is amplitude dependent.

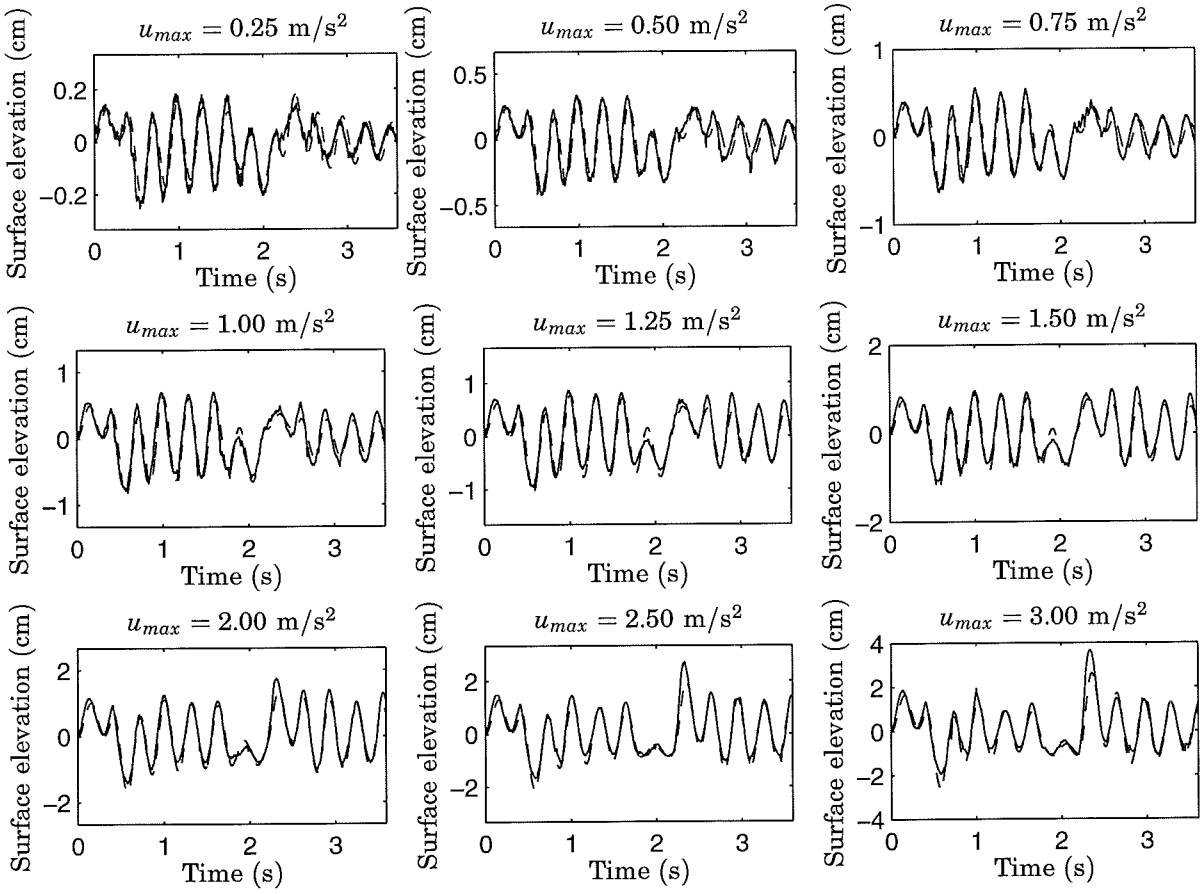

Figure 3.4 Results from experiments with the acceleration profile given in (3.15) for different values of u_{max}. The measured surface elevation (solid) and the estimated surface elevation (dashed).

An easy way to identify the oscillation frequency is to study the free oscillation. The oscillation is started by applying the acceleration profile in (3.14), with $u_{max} = 3$. Figure 3.6 shows the free oscillation from the same experiment as the data in the upper plot of Figure 3.2, the measurement faults are removed and the measurement is low-pass filtered, with bandwidth of 100 rad/s.

The oscillation frequency can be calculated from the time between the zero crossings of the surface elevation. If T_k is the time of the kth zero crossing then the oscillation frequency of the kth half period is given by

$$\omega_k = \frac{4\pi}{T_{k+1} - T_k}$$

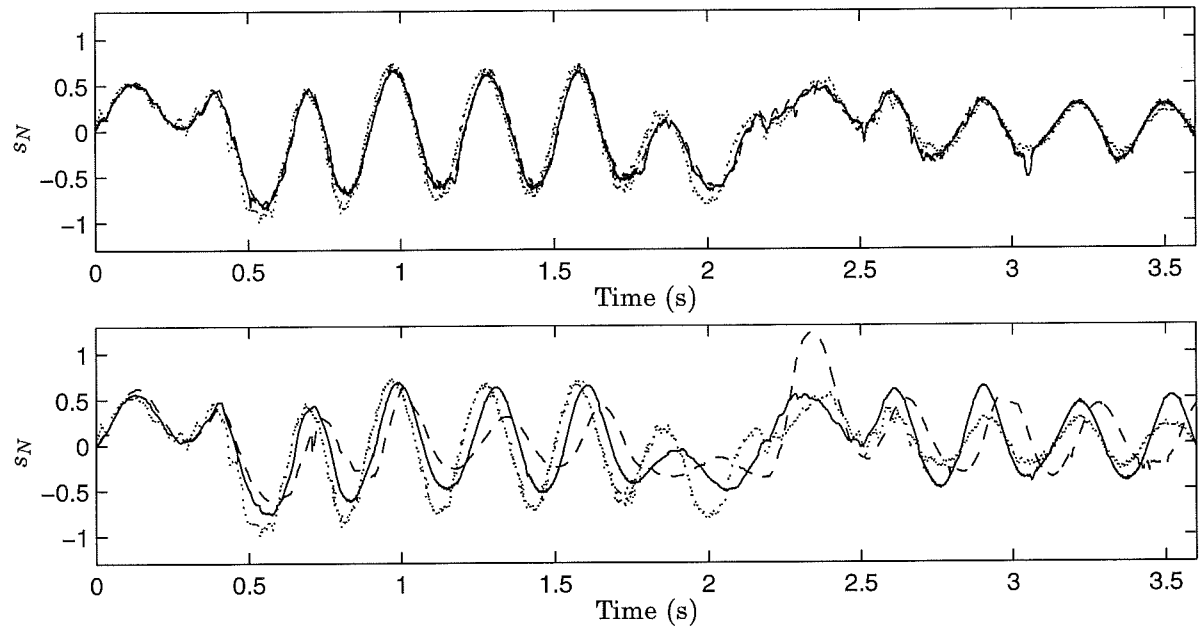

Figure 3.5 The normalized surface elevation; the upper plot shows $u_{max} = 0.25$ m/s^2 (dotted), $u_{max} = 0.50$ m/s^2 (solid) and $u_{max} = 0.75$ m/s^2 (dashed); the lower plot shows $u_{max} = 0.25$ m/s^2 (dotted), $u_{max} = 1.25$ m/s^2 (solid) and $u_{max} = 3.00$ m/s^2 (dashed).

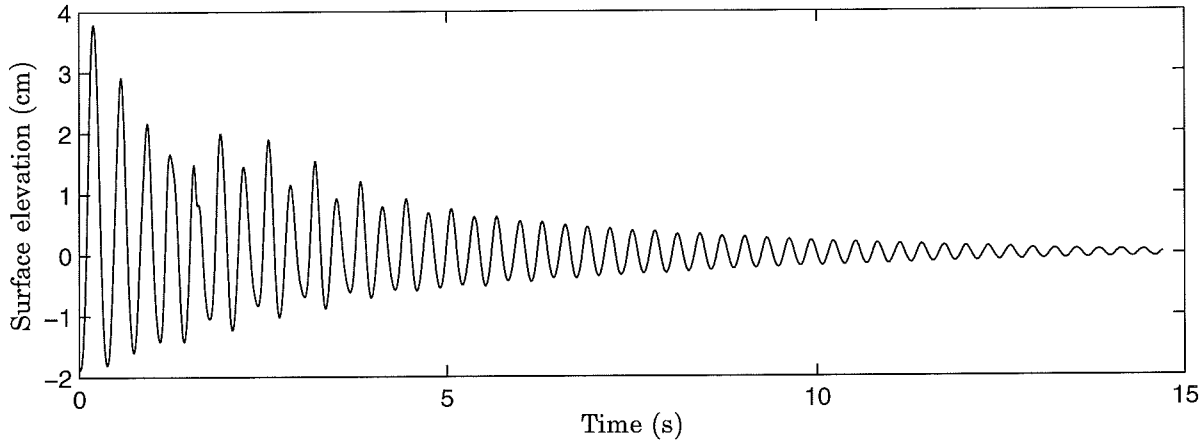

Figure 3.6 The free oscillation when the acceleration profile in (3.14) is used with $u_{max} = 3$. The measurement faults are removed and the measurement is low-pass filtered.

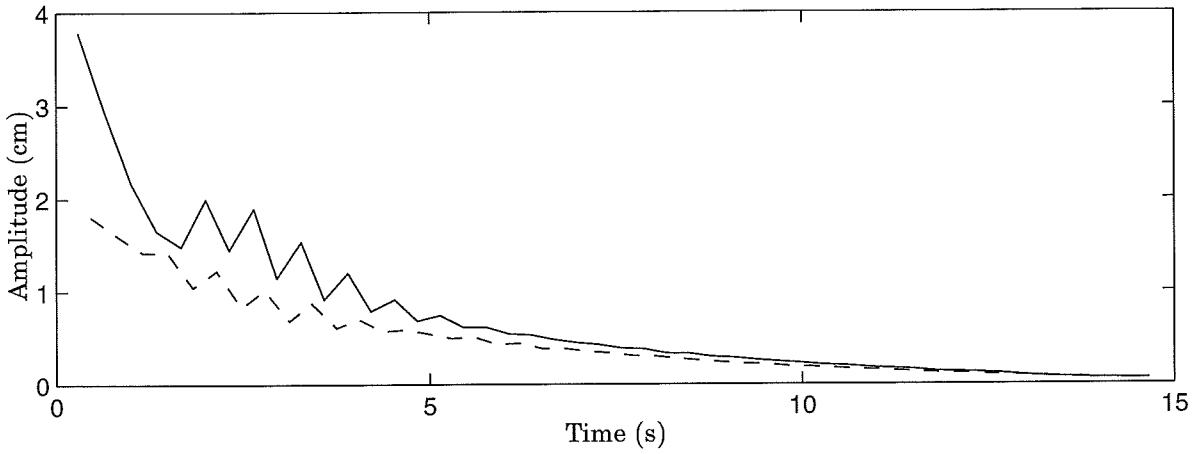

Figure 3.7 The oscillation amplitude as a function of time, positive half periods (solid) and negative half periods (dashed). The oscillation is asymmetric for large amplitudes.

The amplitude of the kth half period is calculated as

$$A_k = \max_{T_k<t<T_{k+1}} |s(t)|$$

where $s(t)$ is the surface elevation. Figure 3.7 shows A_k as a function of T_k for the same experiment as shown in Figure 3.6. In the figure the amplitude of the positive and negative half periods are drawn as two separate lines, this shows that the amplitude of the positive half periods is larger than the amplitude of the negative half periods. This illustrates another nonlinear phenomenon of the slosh, the asymmetric oscillation.

The amplitude dependent oscillation frequency indicated in Table 3.1 can also be seen from the free oscillation. First the amplitude A_k and the oscillation frequency ω_k are made smoother by taking the mean over four half periods to form $\bar{A}_k$ and $\bar{\omega}_k$.

$$\bar{A}_k = \frac{1}{4}\sum_{i=0}^{3} A_{k+i} \ , \qquad \bar{w}_k = \frac{1}{4}\sum_{i=0}^{3} w_{k+i}$$

Figure 3.8 shows $\bar{\omega}_k$ as a function $\bar{A}_k$, the figure clearly shows that the oscillation frequency decreases with increased oscillation amplitude.

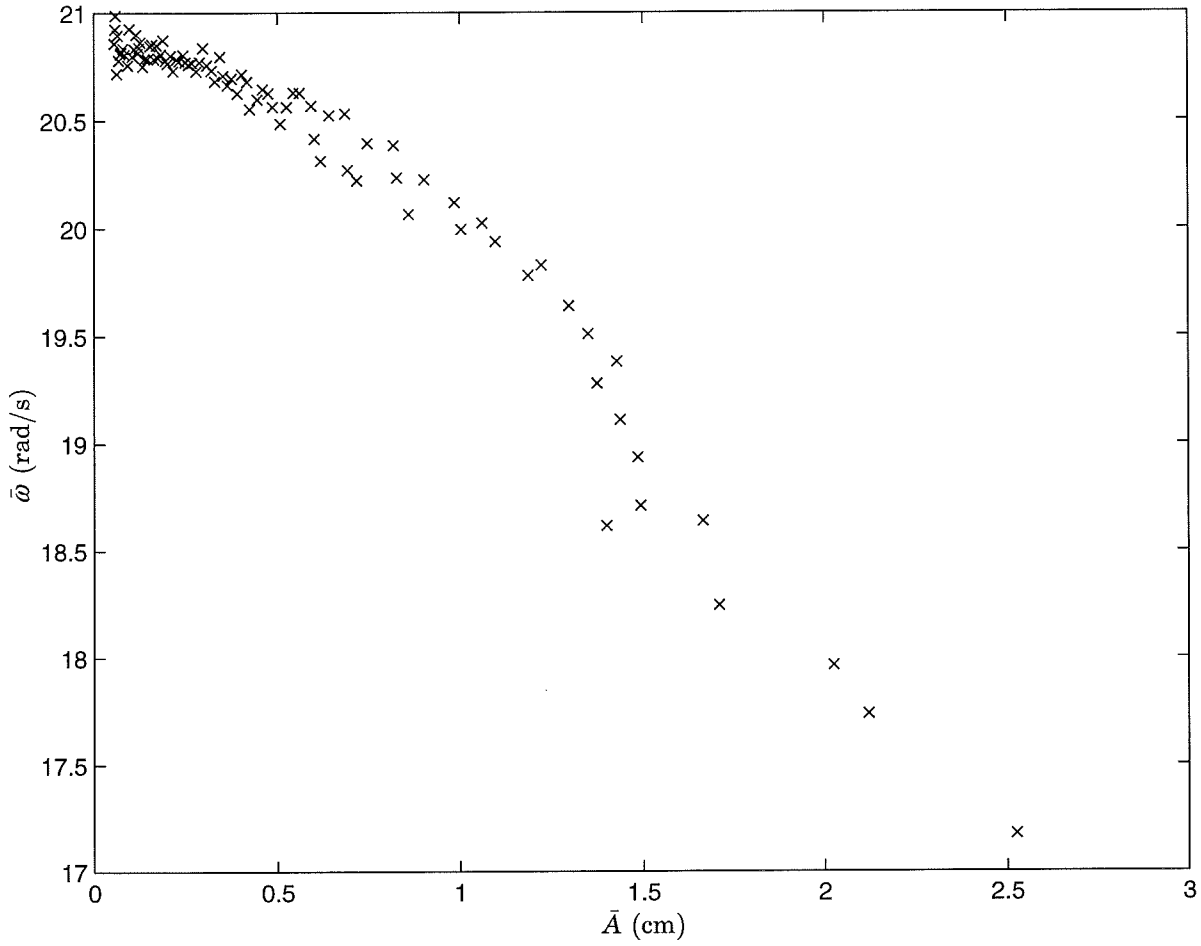

Figure 3.8 The oscillation frequency as a function of the oscillation amplitude.

3.4 The slosh model

The choice of slosh model depends what the model should be used for. If we want to simulate the slosh, an advanced detailed model based on numerical solution of the Navier-Stokes equation is very useful. However, these models are very hard to use for controller design since they are very large and highly nonlinear. For the controller design we would like to have a simple model that captures the most important features of the slosh. If the model is too complex the optimal control problem is very hard to solve.

A simple slosh model

We have chosen to use a simple linear model with four states and found that it captures most of the behavior, two states models the slosh and two states models the motion of the container.

The model is similar to the model proposed by Venugopal and Bernstein (1996) showed in Equation (3.12). Since the higher order modes only have little influence on the surface elevation we only include the first oscillation mode in the model. The direct term is removed and damping is added.

The slosh is modeled by a second order poorly damped system. If we choose the states as: x_2 is the surface elevation and x_1 is the rate of change in the surface elevation divided by the oscillation frequency, the state space representation of the slosh model becomes

$$\begin{bmatrix} \dot{x}_1 \\ \dot{x}_2 \end{bmatrix} = \begin{bmatrix} -2\zeta\omega & -\omega \\ \omega & 0 \end{bmatrix} \begin{bmatrix} x_1 \\ x_2 \end{bmatrix} + \begin{bmatrix} b_1 \\ 0 \end{bmatrix} u \tag{3.17}$$

where ω is the oscillation frequency in radians per second and ζ the relative damping. The parameter b_1 can be determined by studying the stationary gain of the system. If the applied horizontal acceleration is one g the force field affecting the liquid is rotated 45°. In stationarity the liquid surface is flat and orthogonal to the force field, see Figure 3.9. The stationary value of the surface elevation is $a/2$ where a is the container width. Insertion of the stationary values in (3.17) gives

$$\begin{bmatrix} 0 \\ 0 \end{bmatrix} = \begin{bmatrix} -2\zeta\omega & -\omega \\ \omega & 0 \end{bmatrix} \begin{bmatrix} \frac{a}{2} \\ x_2 \end{bmatrix} + \begin{bmatrix} b_1 \\ 0 \end{bmatrix} g \quad \Longrightarrow \quad \begin{cases} x_2 = 0 \\ b_1 = \dfrac{a\omega}{2g} \end{cases}$$

The motion of the container is modeled by a double integrator. If we choose the states as: x_4 is the container position and x_3 is the container velocity, the state space representation of the container motion becomes

$$\begin{bmatrix} \dot{x}_3 \\ \dot{x}_4 \end{bmatrix} = \begin{bmatrix} 0 & 0 \\ 1 & 0 \end{bmatrix} \begin{bmatrix} x_3 \\ x_4 \end{bmatrix} + \begin{bmatrix} 1 \\ 0 \end{bmatrix} u$$

The machine construction is very stiff and the position control is also stiff therfore the motion of the liquid within the container does not

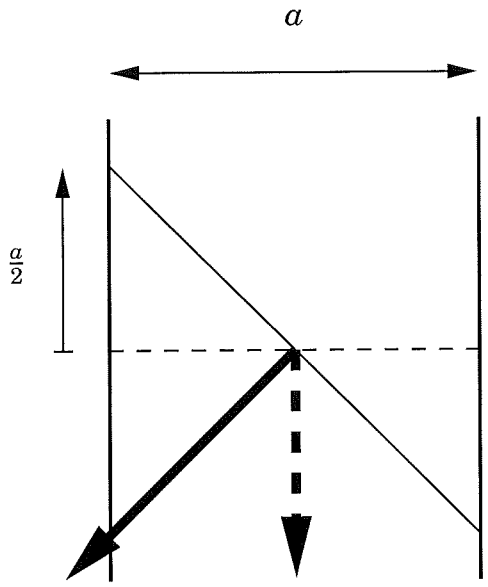

Figure 3.9 Illustration of the container in stationarity. The surface and the direction of the force field with no horizontal acceleration (dashed) and when the container is accelerated with one g.

affect the position of the container. This gives he complete container model

$$\dot{x} = \underbrace{\begin{bmatrix} -2\zeta\omega & -\omega & 0 & 0 \\ \omega & 0 & 0 & 0 \\ 0 & 0 & 0 & 0 \\ 0 & 0 & 1 & 0 \end{bmatrix}}_{A} x + \underbrace{\begin{bmatrix} a\omega/2g \\ 0 \\ 1 \\ 0 \end{bmatrix}}_{B} u \tag{3.18}$$

For a rectangular container with liquid depth h and width a, see Figure 3.10, the oscillation frequency is given by Equation (3.13)

$$\omega = \omega_1 = \sqrt{\frac{g\pi}{a} \tanh \frac{h\pi}{a}}$$

Throughout this thesis a container with $h = 0.2$ m and $a = 0.07$ m is studied, which gives the theoretical value $\omega = 21.0$ rad/s. This is approximatly the same value as the experiments showed for small oscillation amplitudes, see Table 3.1 and Figure 3.8.

For future use we introduce the following definition.

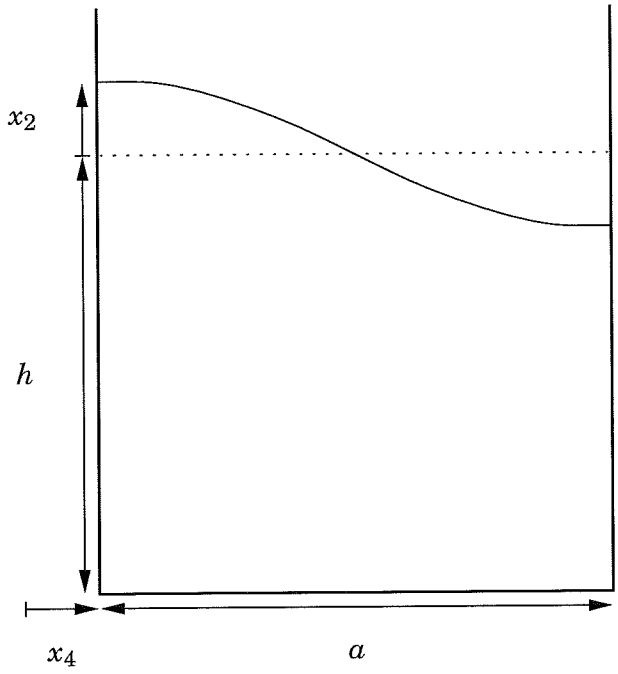

Figure 3.10 Illustration of the container.

DEFINITION 3.1
If $s(t)$ denotes the surface elevation and $\dot{s}(t)$ its time derivative we define the stored internal slosh $s_i(t)$ as

$$s_i(t) = \sqrt{s(t)^2 + \left(\frac{\dot{s}(t)}{w}\right)^2} = \sqrt{x_1(t)^2 + x_2(t)^2}$$

The stored internal slosh represents the amplitude of the oscillation at the time t when $u = 0$, if the damping $\zeta = 0$.

Proof: When $u = 0$ and $\zeta = 0$ the surface elevation can be written as $s(t) = A \sin \omega t$ where A is the oscillation amplitude. Differentiation gives $\dot{s} = \omega A \cos \omega t$. This gives

$$s_i(t) = \sqrt{A^2 \sin^2 \omega t + A^2 \cos^2 \omega t} = A$$

Hence the surface oscillation amplitude. □

4

Calculation of acceleration profiles

This chapter describes different methods for calculating an acceleration profile that meets the specifications. Section 4.1 describes how the problem has been solved in the industry. Related work is presented in Section 4.2. Minimum-time solutions to the problem are given in Sections 4.4 and 4.5, however these accel eration profiles prove to work only for small slosh amplitudes. Therefore, as an alternative, a minimum-energy solution of the problem, which also works for larger slosh amplitudes, is given in Section 4.6. In Section 4.7 an analytical solution is given to a modified version of the minimum-energy problem. Each section contains experimental results with the described acceleration strategy.

4.1 Industrial practice

The acceleration profiles have traditionally been implemented using mechanical devices such as gear boxes and cam discs. This has resulted in very inflexible systems where the acceleration profile can not easily be altered. Therefore, the acceleration profile must be designed such that it fulfills the specifications for the whole range of products. Since the fluid dynamics are very different for different products (compare for example skim milk with yoghurt) this has lead to conservative and non-optimal acceleration profiles.

The recent introduction of servo systems to control the movement offers an increased amount of flexibility. It is now possible to use different acceleration profiles for different products, and it is also possible to tune the acceleration profile for each product. This have given rise to an increased interest in systematic methods for calculation of acceleration profiles.

The solution, up till now, has been to use ad-hoc guessing to determine the structure of the acceleration profile. The development engineers then use exhaustive experiments and experience to tune the parameters. This procedure is very time consuming and therefore it is of great interest to develop methods for calculating good acceleration profiles.

4.2 Related work

A solution to the slosh-free movement problem is suggested in Feddema *et al.* (1997). The approach is based on a second order linear slosh model, similar to the one described in Section 3.4. The acceleration profile is obtained by filtering an acceleration profile that moves the container as fast as possible without any constraints on the slosh. This acceleration profile is given below

$$u(t) = \begin{cases} u_{max} & 0 \leq t < t_s \\ -u_{max} & t_s \leq t < 2t_s \\ 0 & 2t_s \leq t \end{cases} \tag{4.1}$$

where $t_s = \sqrt{\frac{L}{u_{max}}}$. The acceleration profile in (4.1) is the filtered trough the notch-filter given below.

$$G_f(s) = \frac{\sigma^3}{\omega^2} \frac{s^2 + 2\zeta\omega s + \omega^2}{(s+\sigma)^3}$$

where ω and ζ have the same as in the slosh model given in (3.18).

The acceleration strategy is evaluated in experiments with good results. The oscillation frequency of the container is 10.6 rad/s, the

maximum acceleration 0.75 m/s^2, the movement time 2.3 s, the movement distance 0.5 m, and the ratio between the maximum slosh and the container width is 0.04. Compared to our case the maximum acceleration is small, the movement time is long and the ratio between the maximum slosh and the container width is much smaller.

Figure 4.1 shows simulations with this acceleration strategy on our system for some different response speeds of the filter, with $\omega = 21.0$ rad/s, $\zeta = 0$, movement distance 0.2 m. The figure shows that the movement time is considerably increased for $\sigma = 30$ rad/s, and $\sigma = 54$ rad/s gives a very large maximum acceleration. Therefore, this strategy is not feasible when the movement time is in the same range as the oscillation period time.

In Dietze and Schmidt (1997) the problem is solved using optimal control techniques and the same slosh model as presented in Section 3.4. In the optimization the control signal is discretized and the cost function

$$\frac{\alpha^2}{2}[s^2(T) + \dot{s}^2(T)] + \frac{\beta^2}{2}\int_0^T u^2(t)\, dt$$

is numerically minimized for different values of α and β and with constraints on $|u(t)|$ and trajectory constraints on $s(t)$. The problem with $\alpha = 0$, $|u(t)| \leq u_{max}$ and no constraint on the surface elevation $s(t)$ is solved analytically. This approach is very similar to the one presented in Section 4.6.

In Dubois *et al.* (1998) the slosh is modeled by the shallow water equations. The acceleration is calculated using a linearization of the model. Simulations with the nonlinear model show that the acceleration strategy works if the slosh amplitude is small but as the slosh amplitude increases the simulation get more different from the predictions.

Another field that is closely related is anti-swing control of overhead and rotary cranes, see Mårtensson (1972), Gustafsson (1995) and Lee *et al.* (1997). The swinging load is typically modeled as a pendulum. Linearization of the pendulum gives the same model as the one presented in Section 3.4. The main difference is that the angle of the pendulum is measured and used for feedback.

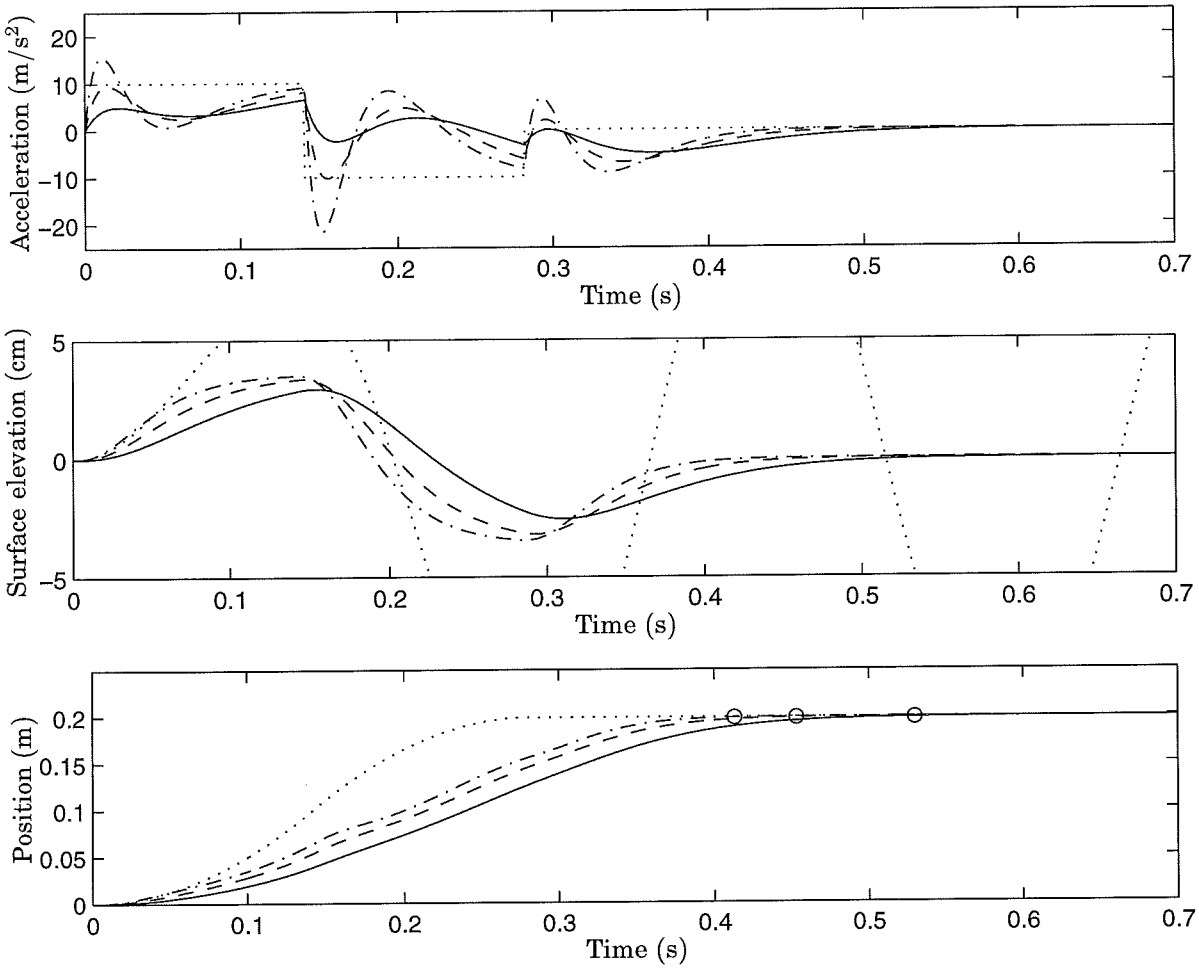

Figure 4.1 Simulations with the notch-filter acceleration profile. Response of the bang-bang acceleration (dotted), $\sigma = 54$ rad/s (dot-dashed), $\sigma = 42$ rad/s (dashed) and $\sigma = 30$ rad/s (solid). The circles in the position diagram show when the position is 0.198 m for the different values of σ.

4.3 Optimal control

Various ways of calculating the acceleration profile are presented in this and the following sections. The acceleration profiles are derived by solving optimal control problems both numerically and analytically. The different strategies are evaluated using experiments.

The control problem

Two problems have been considered and solved:

Movement in several steps

The container is moved the distance $N \cdot L$ in N steps, where N is between 3 and 5. The container should be standing still at the start and in the end of the movement in each step. The same acceleration is applied during every step. During each movement step, the surface elevation must be below a certain level both on both sides of the container. After each movement step, there should be no oscillation in the surface elevation, to ensure that all movement steps start with the same initial conditions.

Movement in one step

The container is moved a distance L standing still at both the start and in the end of the movement. During the movement, the surface elevation must be below a certain level on both sides of the container. After the movement, the surface elevation is allowed to oscillate with a bounded amplitude below the same level as for the surface elevation during the movement.

Constraints

The main constraints used when solving the optimal control problems are

1. Acceleration: $|u(t)| \leq u_{max}$
2. Slosh: $|x_2(t)| \leq s_{max} = 0.035$ m
3. Initial state: $x(0) = [\,0 \quad 0 \quad 0 \quad 0\,]^T$
4. Terminal state:
   (a) Movement in several steps

$$x(T) = [\,0 \quad 0 \quad 0 \quad L\,]^T$$

   (b) Movement in one step

$$s_i(T) = \sqrt{x_1^2(T) + x_2^2(T)} \leq s_{max}$$

$$x_{3:4}(T) = [\,0 \quad L\,]^T$$

where the movement distance $L = 0.2$ m.

4.4 Minimum-time problem

To find an acceleration profile that minimizes the movement time, the following cost function is minimized subject to Constraints 1-4 and the slosh model (3.18)

$$J = \int_0^T 1 \, dt$$

Numerical solution

A numerical solution to the optimal control problem is obtained using a Matlab toolbox called RIOTS (Recursive Integration Optimal Trajectory Solver), see Schwartz and Polak (1996).

RIOTS can only solve fixed time optimal control problems. Therefore, our minimum-time problem has to be transformed to a fixed time problem. This can be done by augmenting the system with a constant state that represent the terminal time. The system now become

$$\begin{aligned} \dot{x} &= [Ax + Bu]z \\ \dot{z} &= 0 \end{aligned}$$

and the cost function

$$J = z(T)$$

If we solve this problem with $T = 1$ the minimum time will be the value of $z(T)$.

The minimum-time solution for the movement in several steps is shown in Figure 4.2 and for the movement in one step in Figure 4.3. The minimum movement times are shown in Table 4.1.

In Figure 4.4 the minimum movement times for different values of u_{max} are shown. As can be seen in the figure when u_{max} is greater than 5 m/s^2 only little decrease in movement time is achieved if u_{max} is increased. Figure 4.5 shows the control signal energy

$$E = \sqrt{\int_0^{T_{opt}} u^2 \, dt}$$

as a function of the minimum movement time. The figure shows that the energy needed for the movement grows very fast when the movement time is decreased.

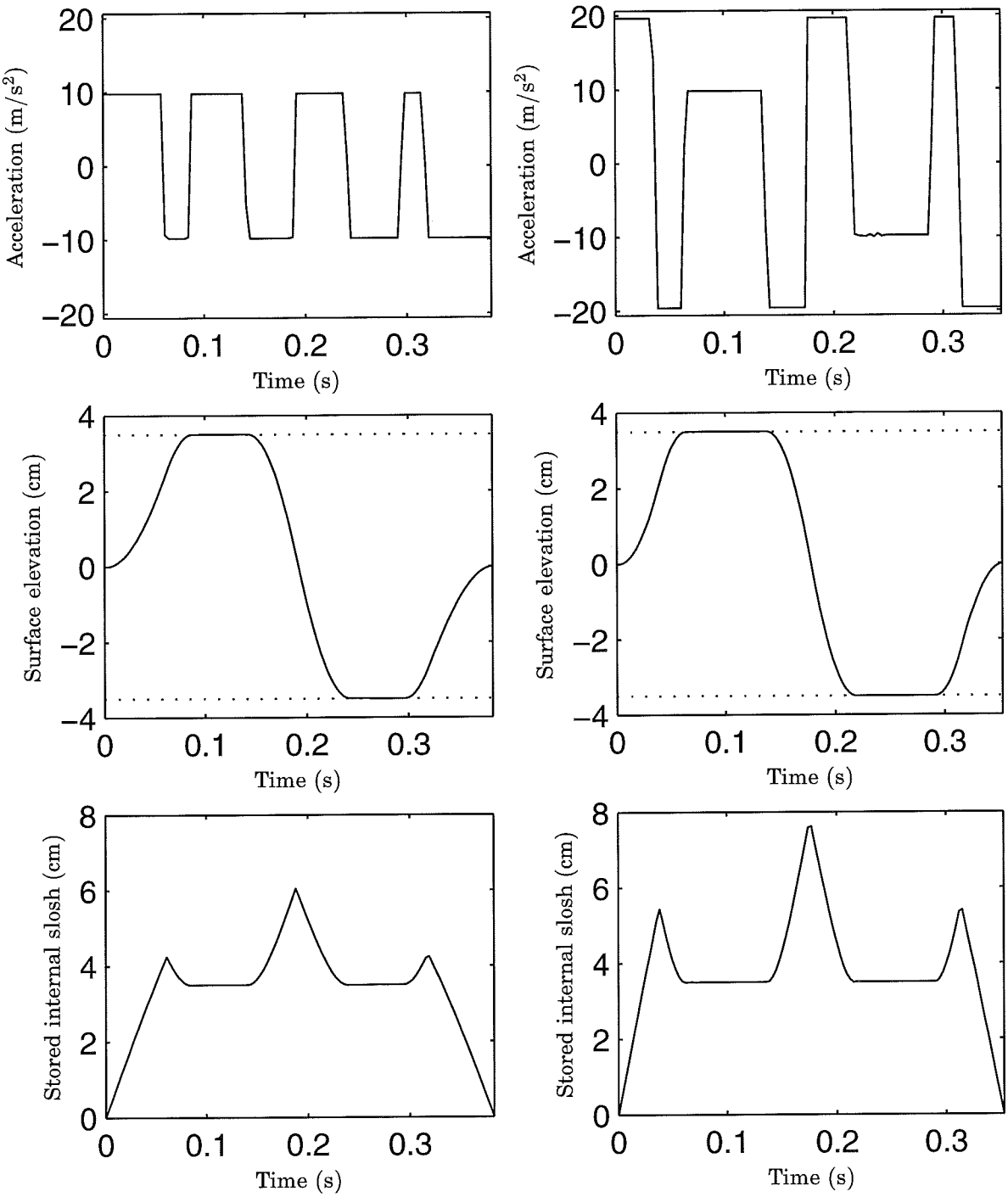

Figure 4.2 Numerical solution of the minimum-time problem for movement in several steps, with $u_{max} = g$ (left) and $u_{max} = 2g$ (right). The movement times are $T = 383$ ms and $T = 353$ ms.

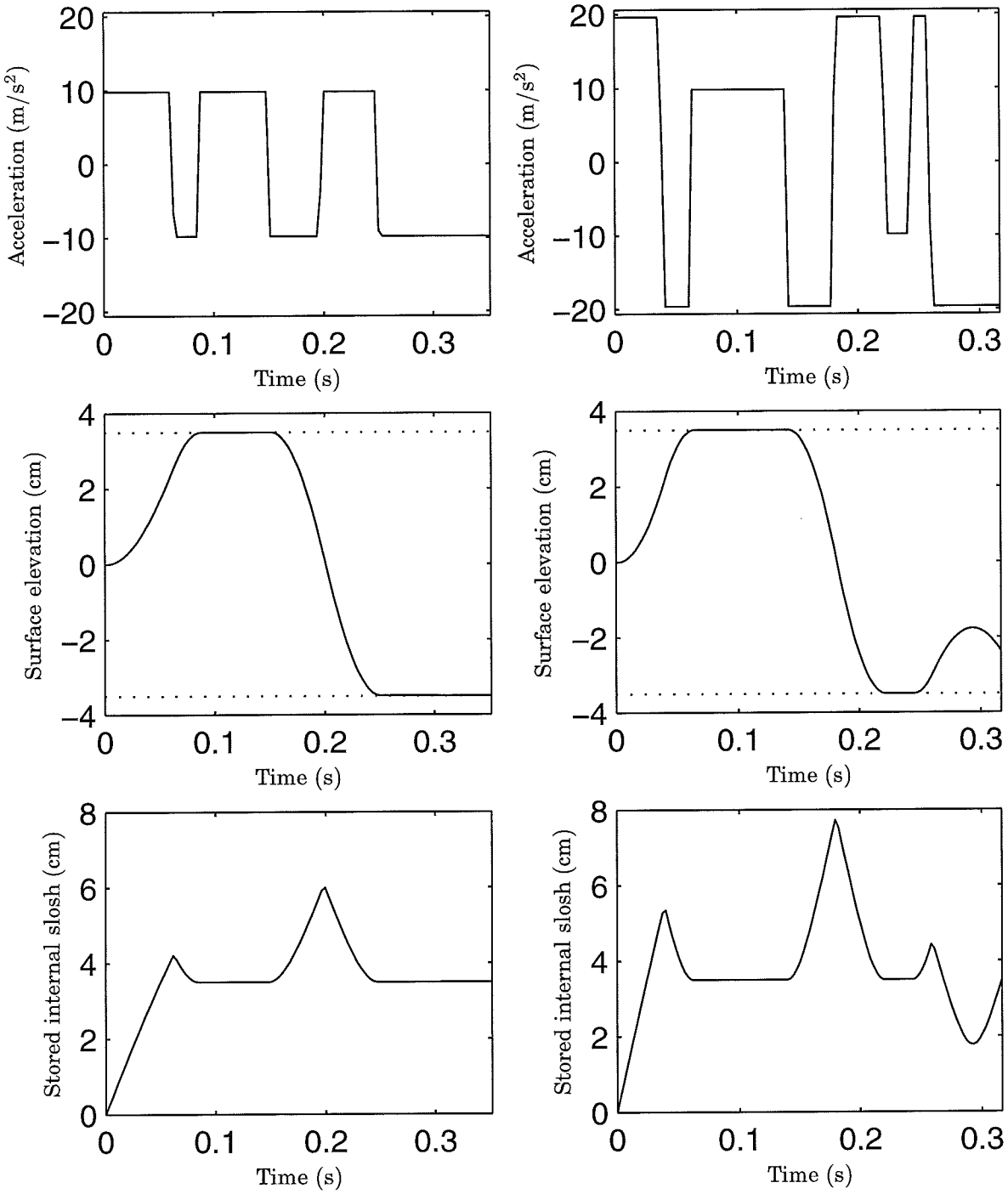

Figure 4.3 Numerical solution of the minimum-time problem for movement in one step, with $u_{max} = g$ (left) and $u_{max} = 2g$ (right).The movement times are $T = 352$ ms and $T = 316$ ms.

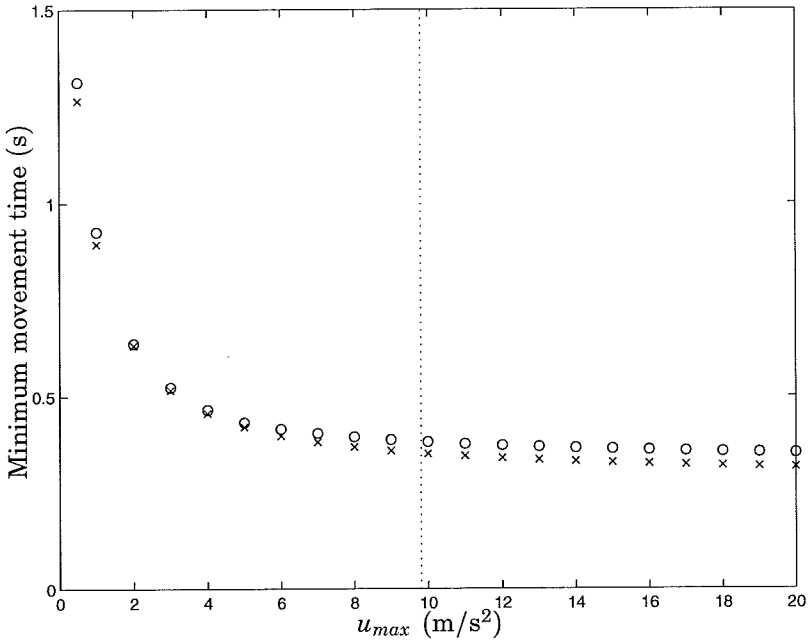

Figure 4.4 The minimum movement time for different values of u_{max}, movement in several steps (∘) and movement in one step (×). The dotted line shows the value of u_{con}.

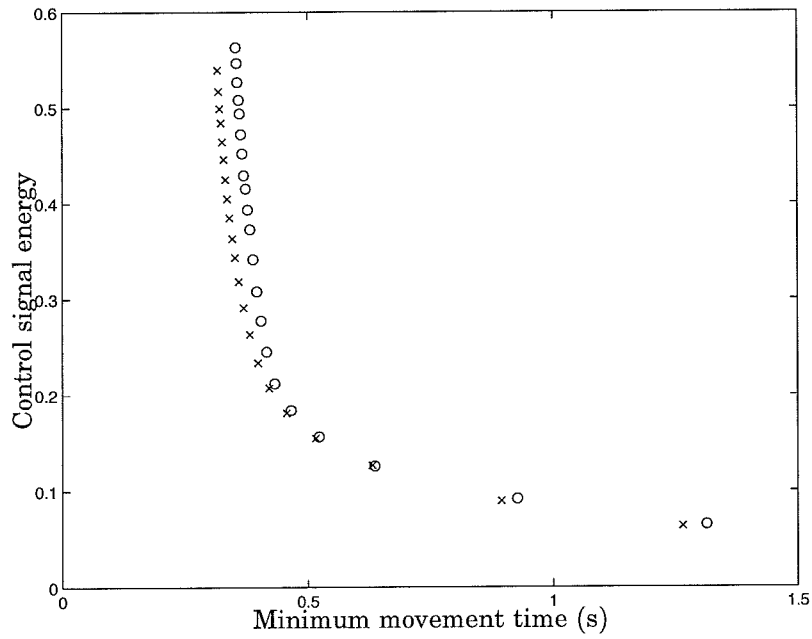

Figure 4.5 The control signal energy as a function of the minimum movement time, movement in several steps (∘) and movement in one step (×).

u_{max}	Movement in several steps	Movement in one step
9.81 m/s^2	383 ms	352 ms
19.62 m/s^2	353 ms	316 ms

Table 4.1 The minimum movement times from the solution of the minimum-time problem, $L = 0.2$ m, $s_{max} = 3.5$ cm and $\omega = 21.0$ rad/s.

Calculation of switching times

Experience shows that if $u_{max} \geq 2s_{max}g/a$ then the time optimal acceleration profile can be divided into five independent operations:

1. Bring the surface up to the level s_{max} as fast as possible with $\dot{s} = 0$ at the end.
2. Keep the surface at level s_{max}.
3. Move the surface from s_{max} to $-s_{max}$ as fast as possible with $\dot{s} = 0$ at the end.
4. Keep the surface at level $-s_{max}$.
5. (a) Movement in several steps
   Bring the surface to 0 as fast as possible with $\dot{s} = 0$ at the end.
   (b) Movement in one step
   Brake the container as fast as possible with the stored internal slosh $s_i = s_{max}$ at the end.

The acceleration profile can in both cases be parameterized as

$$u(t) = \begin{cases} u_{max} & 0 \leq t < t_1 \\ -u_{max} & t_1 \leq t < t_2 \\ u_{con} & t_2 \leq t < t_3 \\ -u_{max} & t_3 \leq t < t_4 \\ u_{max} & t_4 \leq t < t_5 \\ -u_{con} & t_5 \leq t < t_6 \\ u_{max} & t_6 \leq t < t_7 \\ -u_{max} & t_7 \leq t < T \end{cases}$$

where $u_{con} = 2s_{max}g/a$ is the acceleration needed to keep the surface at the constant level s_{max}. For the movement in several steps the switching times can be parameterized as $t_1 = d_1$, $t_2 = t_1 + d_2$, $t_3 = t_2 + d_3$, $t_4 = t_3 + d_4$, $t_5 = t_4 + d_4$, $t_6 = t_5 + d_3$, $t_7 = t_6 + d_2$ and $T = t_7 + d_1$. Now the durations d_1, d_2 and d_4 can be obtained from the solutions of the differential equation

$$\dot{x} = \begin{bmatrix} 0 & -\omega \\ \omega & 0 \end{bmatrix} x + \begin{bmatrix} a\omega/2g \\ 0 \end{bmatrix} u \tag{4.2}$$

where the damping is neglected ($\zeta = 0$).

Solving (4.2) with the boundary values $x(0) = [\,0 \quad 0\,]^T$ and $x(t_2) = [\,0 \quad s_{max}\,]^T$ gives

$$d_1 = \frac{1}{\omega}\arccos\left(2\cos(2d_2) - \frac{u_{max} + u_{con}}{u_{max}}\right) - d_2$$
$$d_2 = \frac{1}{\omega}\arccos\left(\frac{4u_{max}^2 + 2u_{max}u_{con} + u_{con}^2}{4u_{max}^2 + 4u_{max}u_{con}}\right)$$

Solving (4.2) with the boundary values $x(t_3) = [\,0 \quad s_{max}\,]^T$ and $x(t_5) = [\,0 \quad -s_{max}\,]^T$ gives

$$d_4 = \frac{1}{\omega}\arccos\left(\frac{u_{max}}{u_{max} + u_{con}}\right)$$

The duration d_3 is obtained by solving $\ddot{y} = u$ with the boundary values $\dot{y}(0) = 0$, $y(0) = 0$ and $\dot{y}(T) = 0$, $y(T) = L$, which gives

$$d_3 = \frac{1}{u_{con}}\Big(u_{max}(d_2 - d_1) - u_{con}d_4 + [u_{max}^2(d_2 - d_1)^2 + u_{max}u_{con}(d_2^2 - 2d_1d_2 - d_1^2 + d_4^2) + u_{con}^2d_4^2 + u_{con}L]^{\frac{1}{2}}\Big)$$

The calculated switching times corresponds well with the numerical solutions of the problem.

u_{max} (m/s^2)	0.5	1	1.5	2	2.5	3	3.5	4
T (ms)	1361	991	827	729	662	613	575	544

Table 4.2 The minimum movement times for the different values of u_{max}, with $L = 0.2$ m, $s_{max} = au_{max}/(2g)$ and $\omega = 21.0$ rad/s.

Experimental evaluation

Practical evaluations of the minimum-time strategy in the experimental setup have shown that the strategy only works well for small values of s_{max} and u_{max}. For larger values the surface is not a rest at the end of the movement and the maximum slosh is much larger than s_{max}. Since we want to evaluate the strategy when the slosh constraint is active, s_{max} is set to $\frac{a}{2g}u_{max}$. The movement times for the different acceleration profiles are shown in Table 4.2.

Typical results of the experiments are shown in Figure 4.6. The figure shows that for small values of u_{max} the slosh roughly corresponds to the calculated slosh shown in Figure 4.2 except for a high frequency oscillation. However, as u_{max} is increased the performance is drastically degraded.

One reason for this could be the amplitude dependent oscillation frequency, see Section 3.3. To explore this, experiments were done with acceleration profiles calculated for different values of ω. However this lead to no improvement.

Insight into why the performance degrades can be obtained by studying the stored internal slosh s_i shown in Figure 4.2. The figure shows that in the middle of the movement, s_i is first increased and then decreased. This pumping of energy in and out of the system requires a very accurate model to be successful. From Figure 4.6 we also see that the largest deviations appears in the middle of the movement.

4.5 Modified minimum-time problem

To avoid the peaking of the stored internal slosh an extra constraint is added

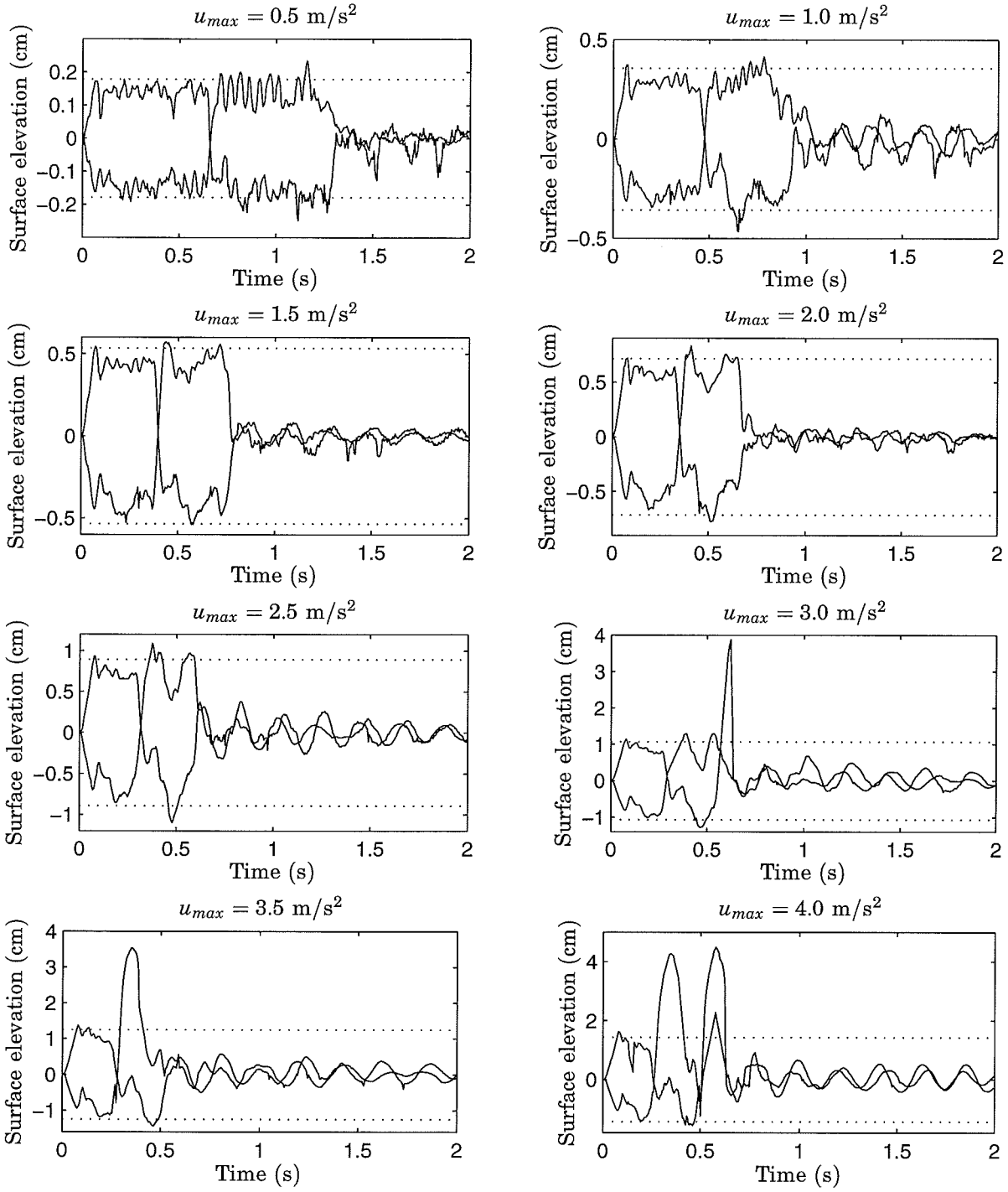

Figure 4.6 Data from experiments with the minimum-time acceleration profile for movement in several steps for varying values of u_{max}.The dotted lines show $\pm s_{max} = \pm \frac{a}{2g} u_{max}$. Each plot shows two experiments, one with the sensor in the front and one with the sensor in the back of the container.

u_{max}	i_{max}	Movement in several steps	Movement in one step
9.81 m/s^2	3.5 cm	390 ms	357 ms
	3.75 cm	387 ms	356 ms
	5.5 cm	383 ms	353 ms
19.62 m/s^2	3.5 cm	368 ms	327 ms
	3.75 cm	364 ms	325 ms
	5.5 cm	354 ms	319 ms

Table 4.3 The minimum movement times from the numerical solution of the modified minimum-time problem, $L = 0.2$ m, $s_{max} = 3.5$ cm and $\omega = 21.0$ rad/s
.

5. Stored internal slosh: $s_i(t) = \sqrt{x_1^2(t) + x_2^2(t)} \leq i_{max}$

The same cost function as in the original minimum-time problem is now minimized subject to Constraints 1-5 and the slosh model.

Numerical solution

The modified minimum-time problem is solved in the same way as the original minimum-time problem. The solution for the movement in several steps is shown in the Figures 4.7, 4.9, 4.11 and for the movement in one step in Figures 4.8, 4.10, 4.12 for different values of i_{max}. The minimum movement times are shown in Table 4.3.

Calculation of switching times

The modified minimum time acceleration profile is built up by the same five independent operations as the original minimum time acceleration profile, but experience shows that each operation is divided into sub operations:

1. Bring the surface up to the level s_{max} as fast as possible with $\dot{s} = 0$ at the end.

   i Bring the stored internal slosh up to i_{max}.

   ii Keep the stored internal slosh at i_{max}.

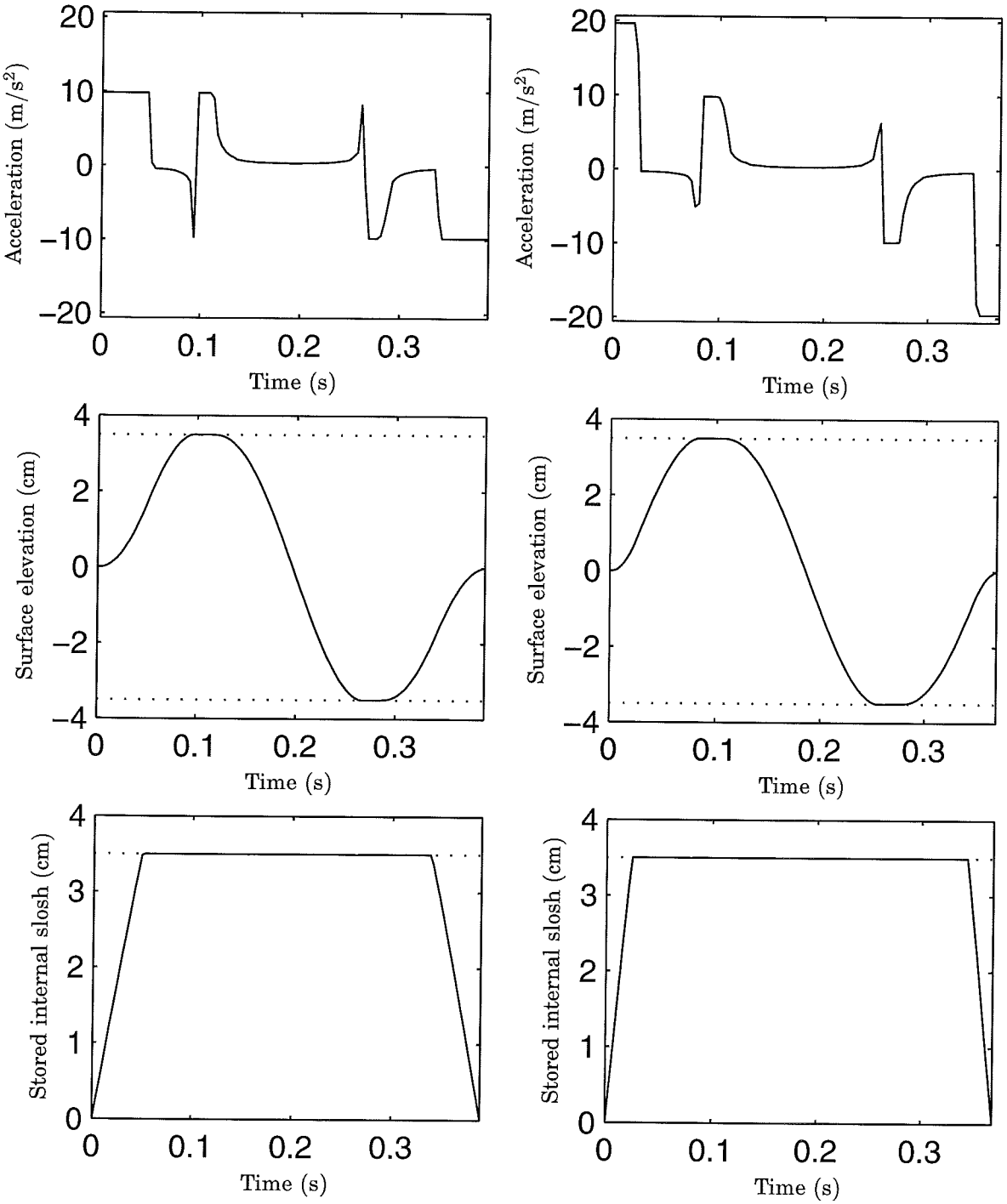

Figure 4.7 Numerical solution of the modified minimum-time problem for movement in several steps, with $i_{max} = 3.5$ cm, $u_{max} = g$ (left) and $u_{max} = 2g$ (right). The movement times are $T = 390$ ms and $T = 368$ ms. The dotted line show the value of s_{max} and i_{max}.

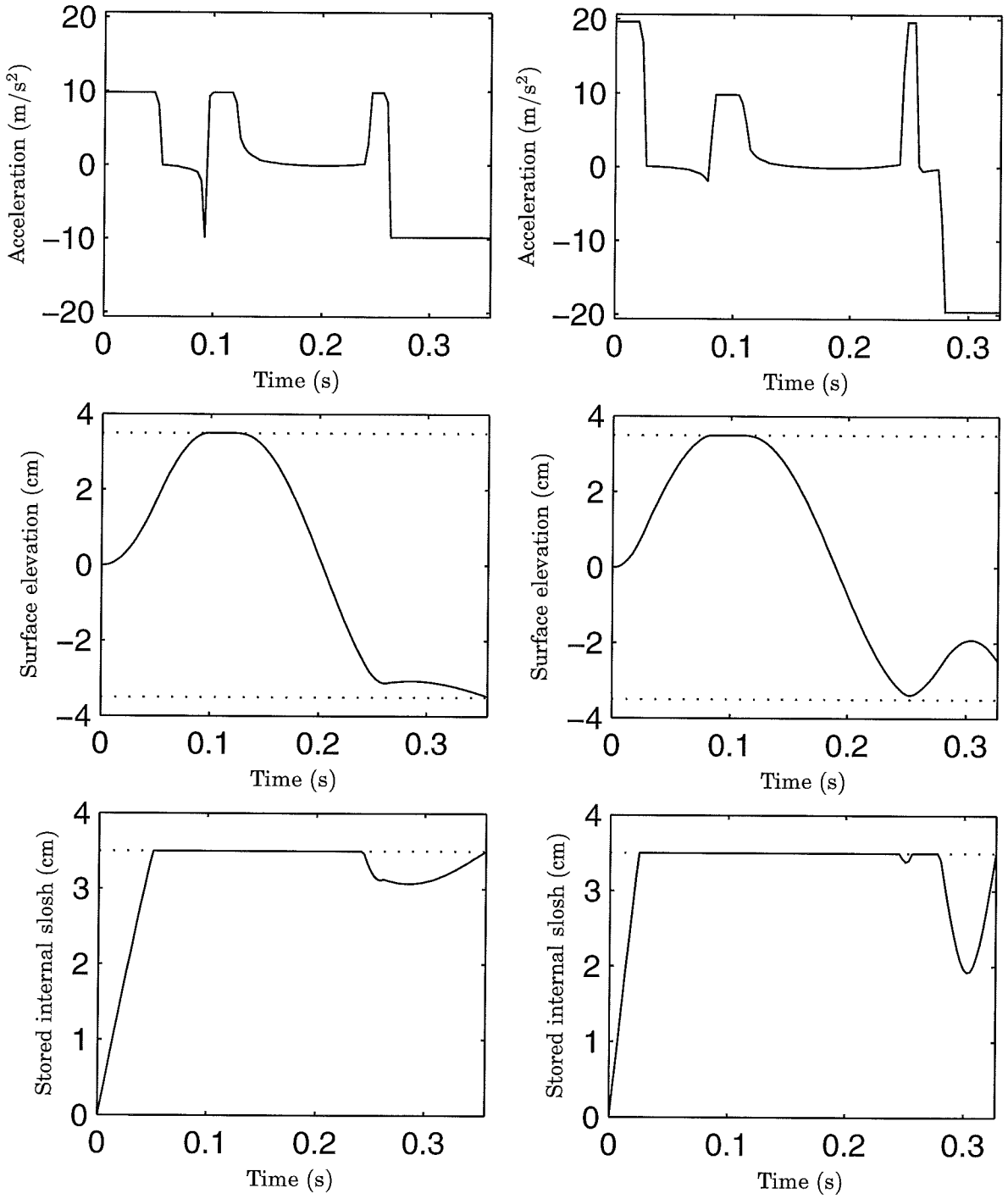

Figure 4.8 Numerical solution of the modified minimum-time problem for movement in one step, with $i_{max} = 3.5$ cm, $u_{max} = g$ (left) and $u_{max} = 2g$ (right).The movement times are $T = 357$ ms and $T = 337$ ms. The dotted line show the value of s_{max} and i_{max}.

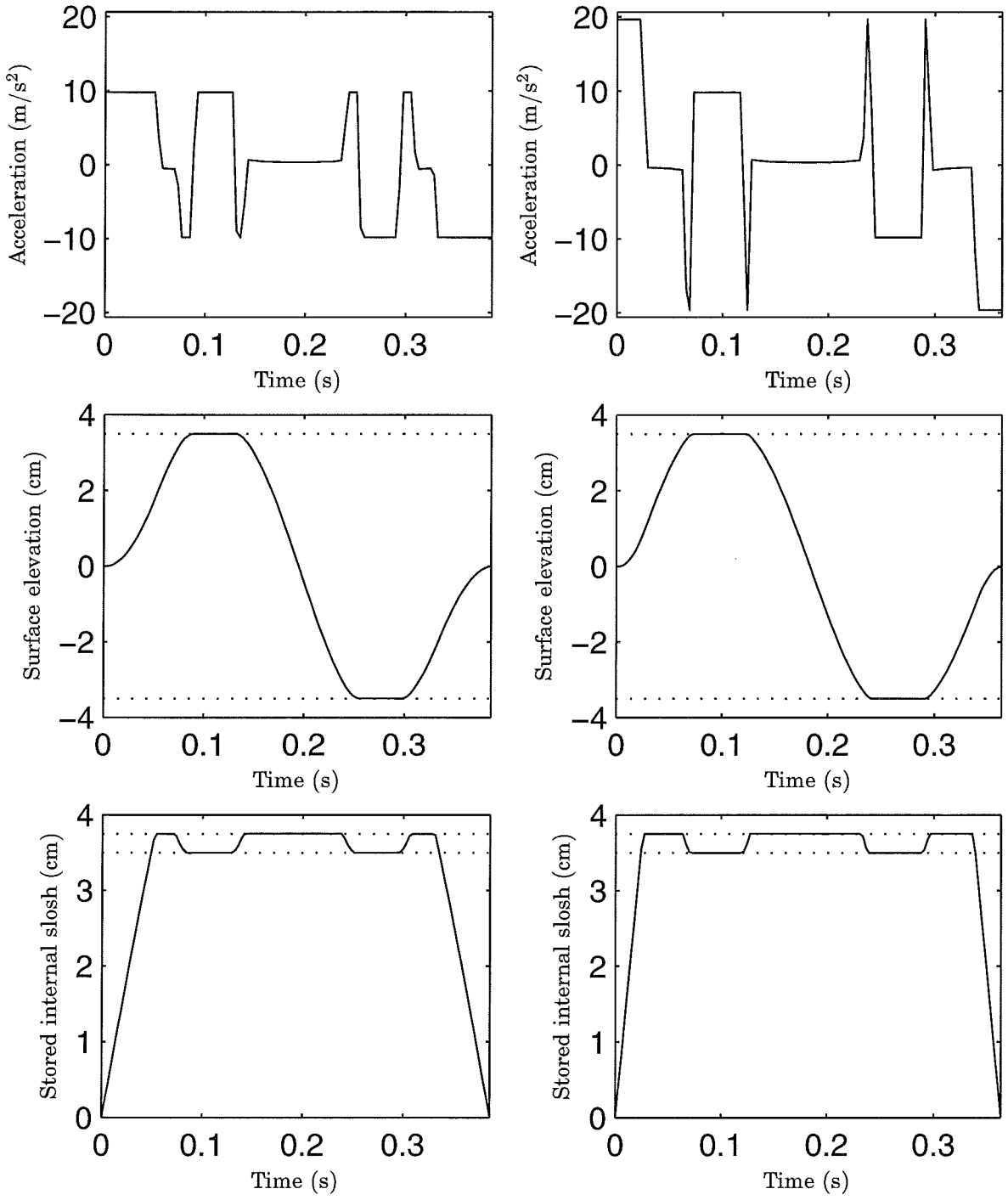

Figure 4.9 Numerical solution of the modified minimum-time problem for movement in several steps, with $i_{max} = 3.75$ cm, $u_{max} = g$ (left) and $u_{max} = 2g$ (right). The movement times are $T = 387$ ms and $T = 364$ ms. The dotted lines show the values of s_{max} and i_{max}.

and $u_{max} = 2g$ (right).The movement times are $T = 353$ ms and

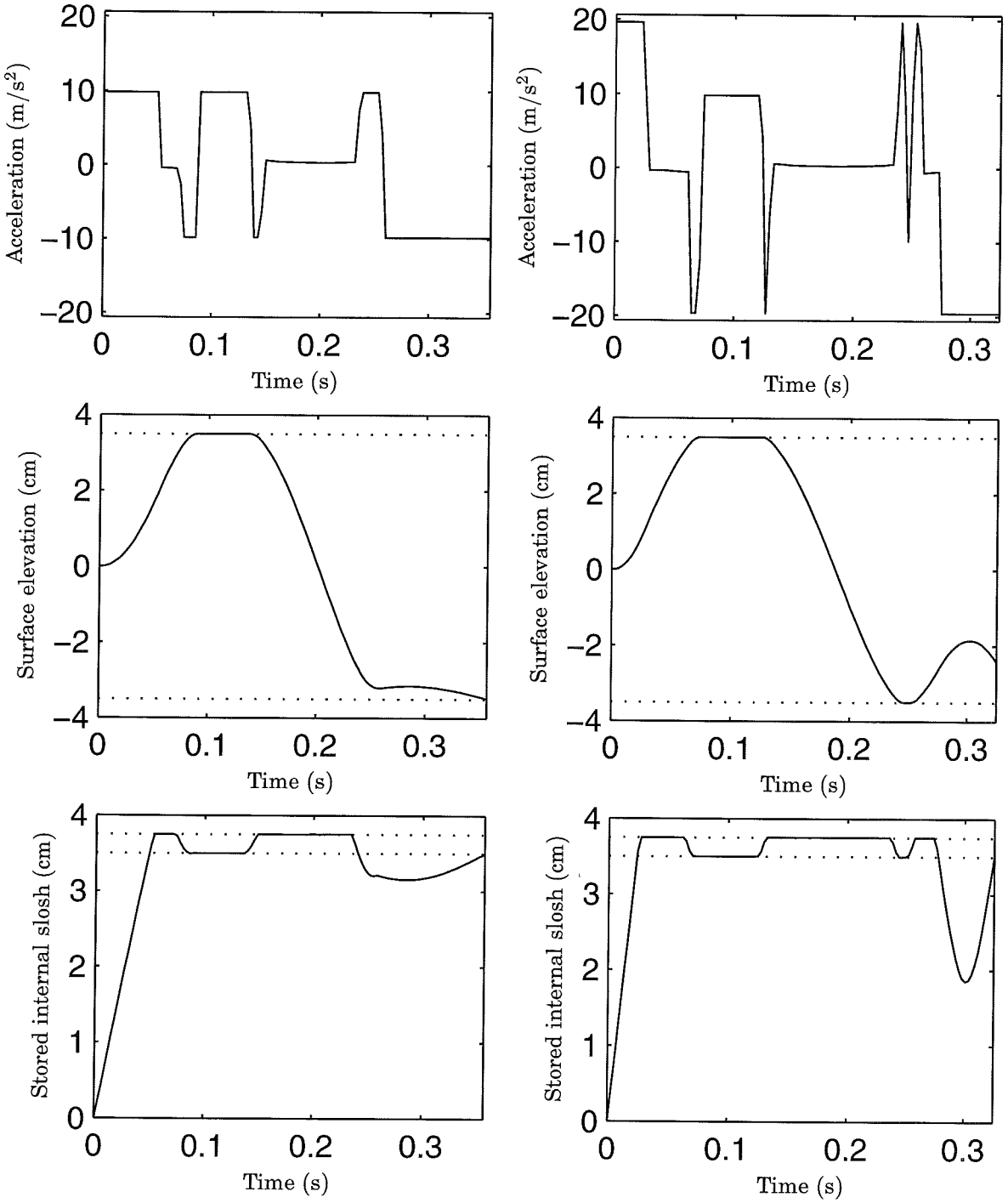

Figure 4.10 Numerical solution of the modified minimum-time problem for movement in one step, with $i_{max} = 3.75$ cm, $u_{max} = g$ (left) and $u_{max} = 2g$ (right).The movement times are $T = 356$ ms and $T = 325$ ms. The dotted lines show the values of s_{max} and i_{max}.

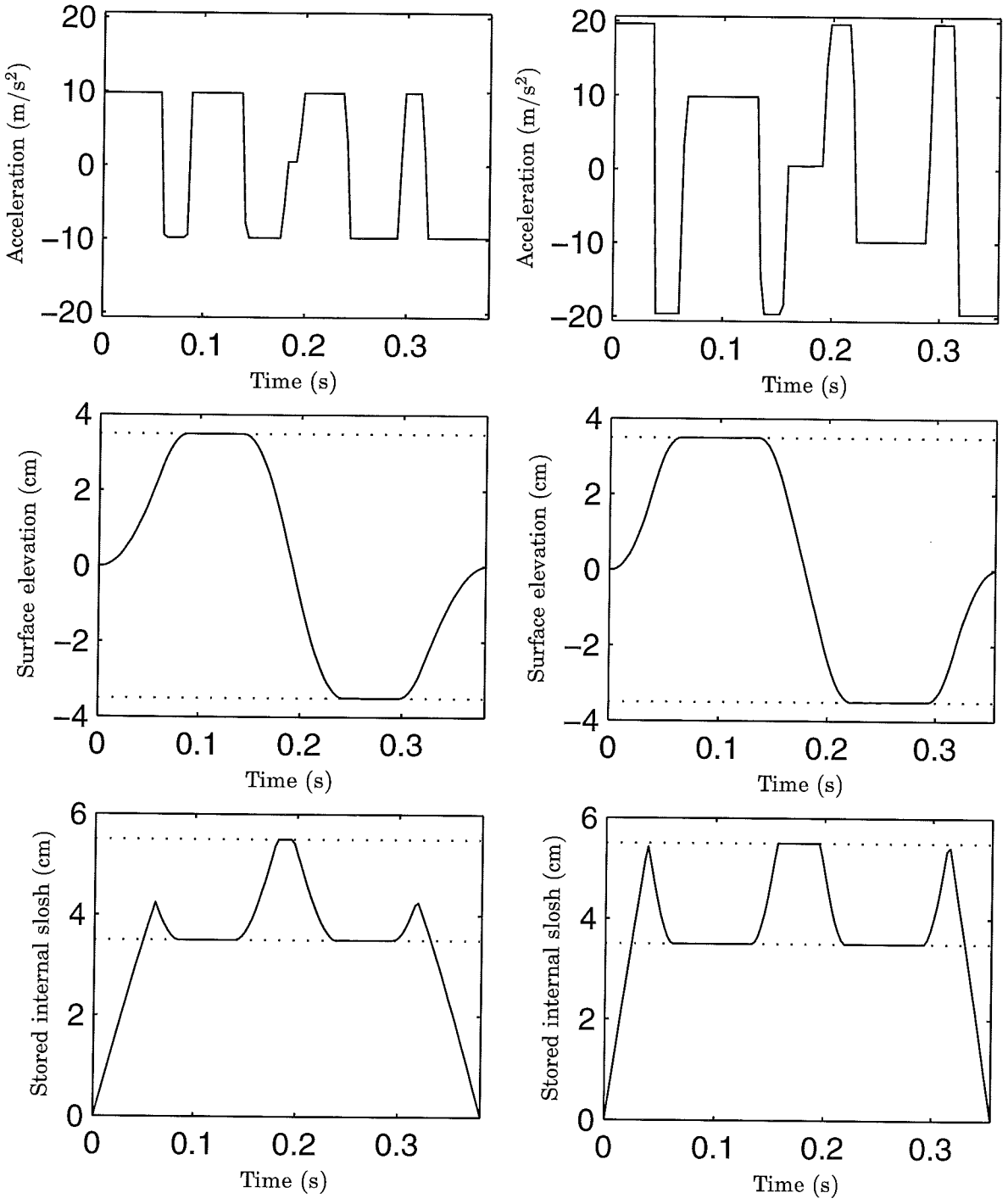

Figure 4.11 Numerical solution of the modified minimum-time problem for movement in several steps, with $i_{max} = 5.5$ cm, $u_{max} = g$ (left) and $u_{max} = 2g$ (right). The movement times are $T = 383$ ms and $T = 354$ ms. The dotted lines show the values of s_{max} and i_{max}.

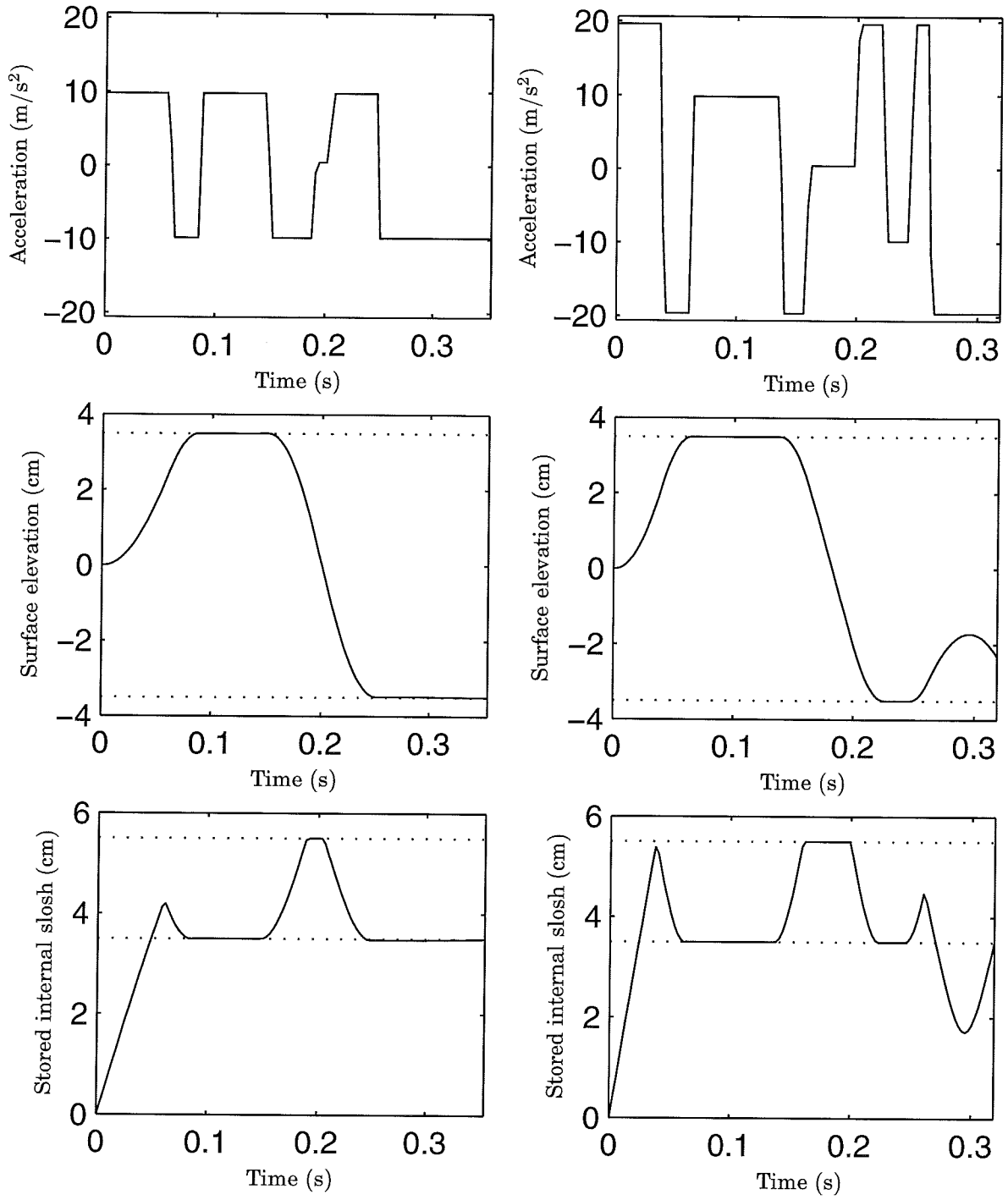

Figure 4.12 Numerical solution of the modified minimum-time problem for movement in one step, with $i_{max} = 5.5$ cm, $u_{max} = g$ (left) and $u_{max} = 2g$ (right).The movement times are $T = 353$ ms and $T = 319$ ms. The dotted lines show the values of s_{max} and i_{max}.

iii Bring the surface up to s_{max} and bring the stored internal slosh down to s_{max}.

2. Keep the surface at level s_{max}.

3. Move the surface from s_{max} to $-s_{max}$ as fast as possible with $\dot{s} = 0$ at the end.

   i Bring the stored internal slosh up to i_{max}.

   ii Keep the stored internal slosh at i_{max}.

   iii Bring the surface down to $-s_{max}$ and the stored internal slosh down to s_{max}.

4. Keep the surface at level $-s_{max}$.

5. a Movement in one step:
   Brake the container as fast as possible with the stored internal slosh $s_i = s_{max}$ at the end.

   b Movement in several steps:
   Bring the surface to 0 as fast as possible with $\dot{s} = 0$ at the end.

   i. Bring the stored internal slosh up to i_{max}.

   ii. Keep the stored internal slosh at i_{max}.

   iii. Bring the surface up to 0 and the stored internal slosh down to 0.

The modified time optimal acceleration profile can in both cases be

parameterized as

$$u(t) = \begin{cases} u_{max} & 0 \le t < t_1 \\ u_i(\dot{s}) & t_1 \le t < t_2 \\ -u_{max} & t_2 \le t < t_3 \\ u_{con} & t_3 \le t < t_4 \\ -u_{max} & t_4 \le t < t_5 \\ u_i(\dot{s}) & t_5 \le t < t_6 \\ u_{max} & t_6 \le t < t_7 \\ -u_{con} & t_7 \le t < t_8 \\ u_{max} & t_8 \le t < t_9 \\ u_i(\dot{s}) & t_9 \le t < t_{10} \\ -u_{max} & t_{10} \le t < T \end{cases}$$

where $u_{con} = 2s_{max}g/a$ is the acceleration needed to keep the surface at a constant level and $u_i(\dot{s})$ is the control signal needed to keep the stored internal slosh s_i at a constant level when the surface is moving and $\dot{s}$ is the time derivative of the surface elevation. An expression for $u_i(\dot{s})$ is obtained from the time derivative of the stored internal slosh.

$$\dot{s}_i = \frac{1}{s_i}\left(s(t)\dot{s}(t) + \frac{\dot{s}(t)\ddot{s}(t)}{w^2}\right)$$

Since we are interested in the case when s_i is constant we get

$$s(t)\dot{s}(t) + \frac{\dot{s}(t)\ddot{s}(t)}{w^2} = 0$$

Insertion of $\ddot{s} = -2\zeta\omega\dot{s} - \omega^2 s - a\omega^2 u/(2g)$ gives

$$-\frac{1}{g\omega}\dot{s}(t)(4\zeta g\dot{s}(t) + a\omega u(t)) = 0$$

since $\dot{s} \neq 0$ hence $u_i(\dot{s}) = 4\zeta g\dot{s}/(a\omega)$.

For the movement in several steps the switching times are again symmetric and can be parameterized as $t_1 = d_1$, $t_2 = t_1 + d_2$, $t_3 = t_2 + d_3$,

$t_4 = t_3 + d_4$, $t_5 = t_4 + d_5$, $t_6 = t_5 + d_6$, $t_7 = t_6 + d_5$, $t_8 = t_7 + d_4$, $t_9 = t_8 + d_3$, $t_{10} = t_9 + d_2$ and $T = t_{10} + d_1$. For the case when $i_{max} = s_{max}$ and $\zeta = 0$ the switching times can be calculated in the same way as for the original minimum time problem and are then given by

$$
\begin{aligned}
d_1 &= \frac{2}{\omega} \arctan\left(\frac{u_{con}}{\sqrt{4u_{max}^2 - u_{con}^2}}\right) \\
d_2 &= \frac{1}{\omega} \arccos\left(\frac{u_{con}}{2u_{max}}\right) \\
d_3 &= 0 \\
d_4 &= \frac{1}{2u_{con}}(-2u_{max}d_1 - u_{con}d_6 + \\
&\qquad [4u_{max}^2 d_1^2 - 4u_{max}u_{con}(d_1^2 + 2d_1d_2) + u_{con}^2 d_4^2 + 4u_{con}L]^{\frac{1}{2}}) \\
d_5 &= 0 \\
d_6 &= \frac{\pi}{\omega}
\end{aligned}
$$

The switching times when $i_{max} > s_{max}$ are harder to calculate analytically.

Experimental evaluation

The evaluation of the modified minimum-time acceleration profiles was done in the same way as for the original minimum-time acceleration profiles, with $s_{max} = i_{max} = \frac{a}{2g}u_{max}$ to ensure that the constraints are active. The minimum movement times are shown in Table 4.4 and typical results from the experiments are shown in Figure 4.13.

A comparison with the experimental results with the profiles obtained from the original minimum-time problem, shown in Figure 4.6, reveals that larger values of u_{max} and s_{max} can be used before the performance degrades.

In an attempt to improve the performance, acceleration profiles calculated for different values of ω were tested. However this lead to no improvement.

A conclusion that can be drawn is that limiting the stored internal slosh has a positive effect and the minimum movement times are only slightly increased compared to the original minimum-time problem.

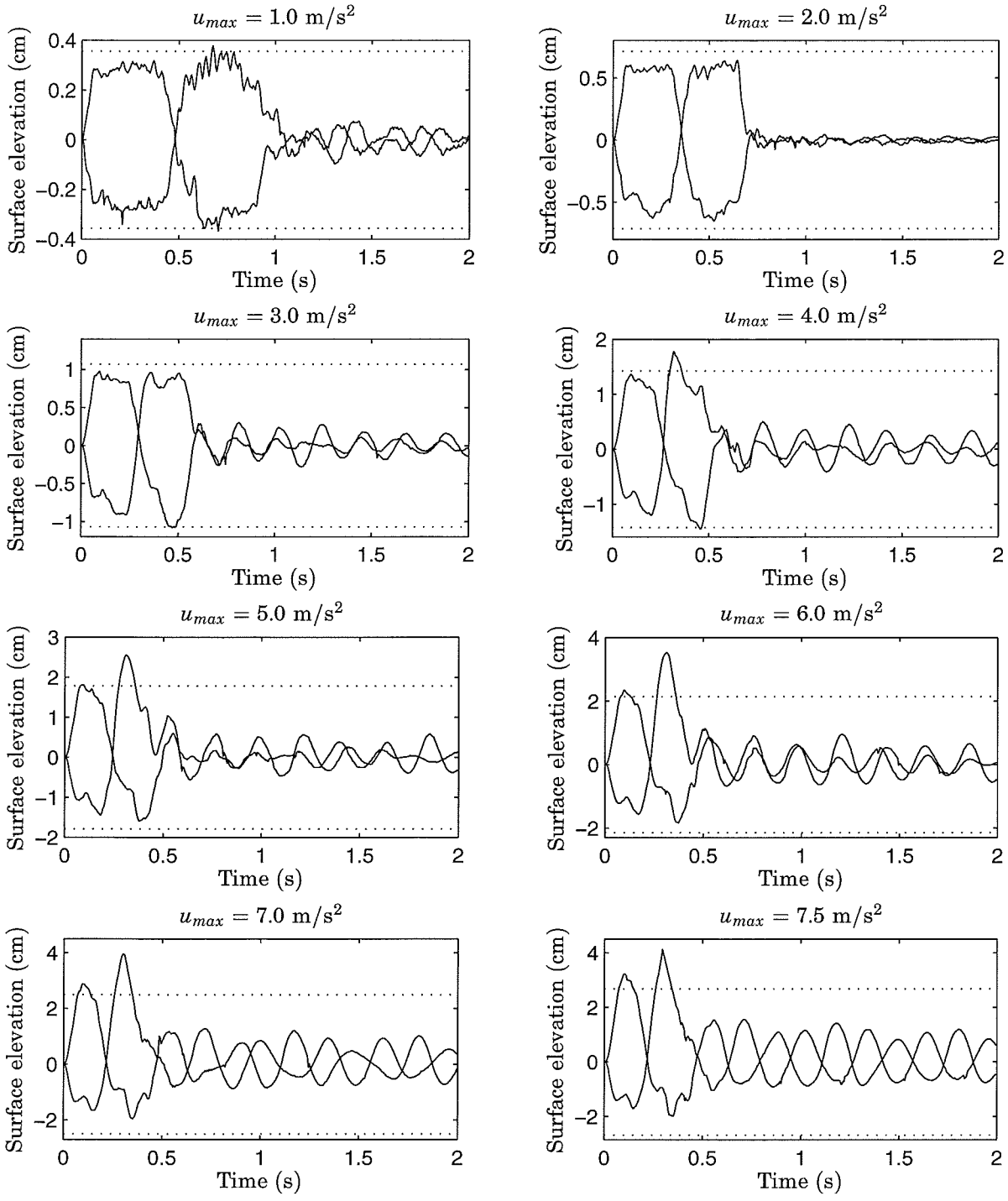

Figure 4.13 Data from experiments with the modified minimum-time acceleration profile for movement in several steps for varying values of u_{max}. The dotted lines shows $\pm s_{max} = \pm i_{max} = \pm\frac{a}{2g}u_{max}$. Each plot shows two experiments, one with the sensor in the front and one with the sensor in the back of the container. Compared with Figure 4.6 larger values of u_{max} can be used before the performance degrades.

u_{max} (m/s^2)	1	2	3	4	5	6	7	7.5
T (ms)	995	734	618	550	503	468	441	430

Table 4.4 The minimum movement times for the different values of u_{max} for the modified minimum-time acceleration profiles, with $L = 0.2$ m, $i_{max} = s_{max} = au_{max}/(2g)$ cm and $\omega = 21.0$ rad/s. The movement time is only slightly increased compared to the movement times for the original minimum-time problem in Table 4.2.

The acceleration profiles are however still useless for fast movements.

4.6 Minimum-energy problem

One way of making the acceleration profile smoother is to solve a minimum-energy problem instead. The cost function

$$J = \int_0^{T_{opt}+\Delta} u^2(t)\, dt$$

is minimized subject to the Constraints 1-4 and the slosh model (3.18), where T_{opt} is the time from the solution of the minimum-time problem and Δ is the extra time we can allow for the movement.

Numerical solution

The problem is solved numerically and the result for the movement in several steps is shown in Figure 4.14 and for the movement in one step in Figure 4.15 for different values of Δ. The figures show that by increasing the movement time slightly we can make the acceleration profile much smoother. Notice that when Δ is sufficiently large neither the control nor the control constraint is active.

Experimental evaluation

The minimum-energy acceleration profiles are evaluated for different values of Δ and ω with $u_{max} = 9.81$ m/s^2 and $s_{max} = 3.5$ cm. Table 4.5 shows the movement times and the relative increase in movement time

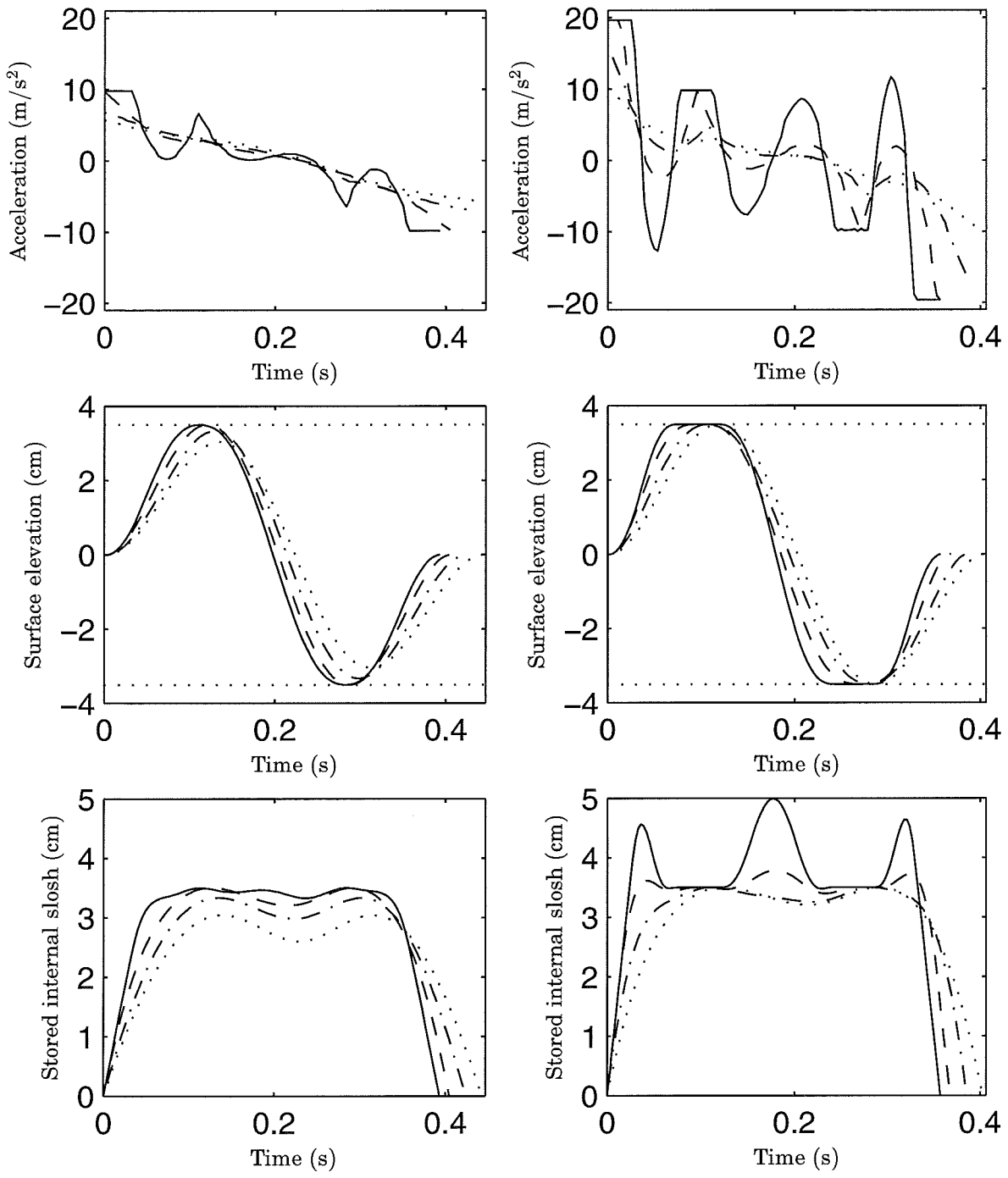

Figure 4.14 Numerical solution of the minimum-energy problem for movement in several steps with $u_{max} = g$ (left) and $u_{max} = 2g$ (right) for different values of Δ, $\Delta = 0.02T_{opt}$ (solid), $\Delta = 0.05T_{opt}$ (dashed), $\Delta = 0.10T_{opt}$ (dash dotted) and $\Delta = 0.15T_{opt}$ (dotted).

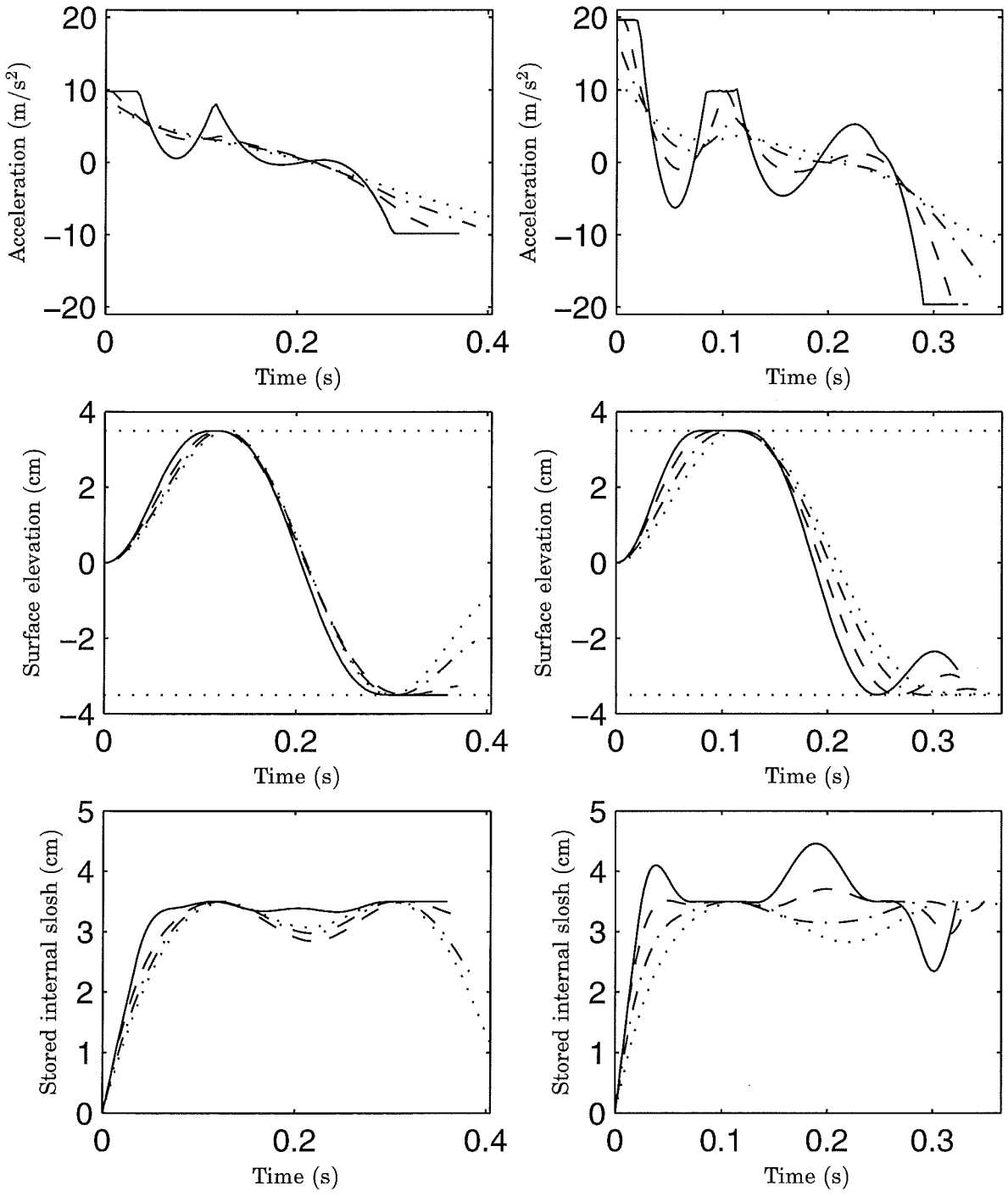

Figure 4.15 Numerical solution of the minimum-energy problem for movement in one step with $u_{max} = g$ (left) and $u_{max} = 2g$ (right) for different values of Δ, $\Delta = 0.02T_{opt}$ (solid), $\Delta = 0.05T_{opt}$ (dashed), $\Delta = 0.10T_{opt}$ (dash dotted) and $\Delta = 0.15T_{opt}$ (dotted).

	T (ms)	417	444	478	520	570
$\omega = 21.0$ rad/s	Δ/T_{opt} (%)	9	16	25	36	49
$T_{opt} = 383$ ms	max u (m/s^2)	7.35	5.73	4.58	4.03	3.97
	max s (cm)	3.47	3.05	2.58	2.06	1.63
$\omega = 19.5$ rad/s	Δ/T_{opt} (%)	7	14	23	33	46
$T_{opt} = 390$ ms	max u (m/s^2)	8.81	6.65	4.95	3.86	3.44
	max s (cm)	3.43	3.05	2.63	2.17	1.69
$\omega = 18.0$ rad/s	Δ/T_{opt} (%)	5	11	20	30	43
$T_{opt} = 399$ ms	max u (m/s^2)	9.81	8.14	5.82	4.15	3.21
	max s (cm)	3.42	3.02	2.63	2.22	1.79

Table 4.5 The relative increase in movement time, the maximum of the applied acceleration and the calculated maximum slosh are shown for different values of the movement time T and different ω from the numerical solution of the problem.

for different values of ω. The acceleration profiles are calculated for five movement times T and three values of ω.

Since the minimum movement time T_{opt} depends on ω, the relative increase in movement time is different for the different values of ω. The results of the experiments are shown in Figure 4.16. In the plots for $\omega = 21.0$ rad/s, $T = 417$ ms and $T = 444$ ms, the sensor was not able to measure the surface elevation between $t \approx 0.5$ s and $t \approx 0.7s$, this resulted in the straight lines in the plots.

Figure 4.16 shows that the performance can be increased by adjusting the value of ω. When $T = 570$ ms the best performance is achieved with $\omega = 21.0$ rad/s, for $T = 478$ ms $\omega = 19.5$ rad/s gives the best performance and $\omega = 18.0$ rad/s gives the best performance when $T = 417$ ms. If performance is defined as the amplitude of the surface oscillations after the movement is performed, the smaller amplitude the better performance.

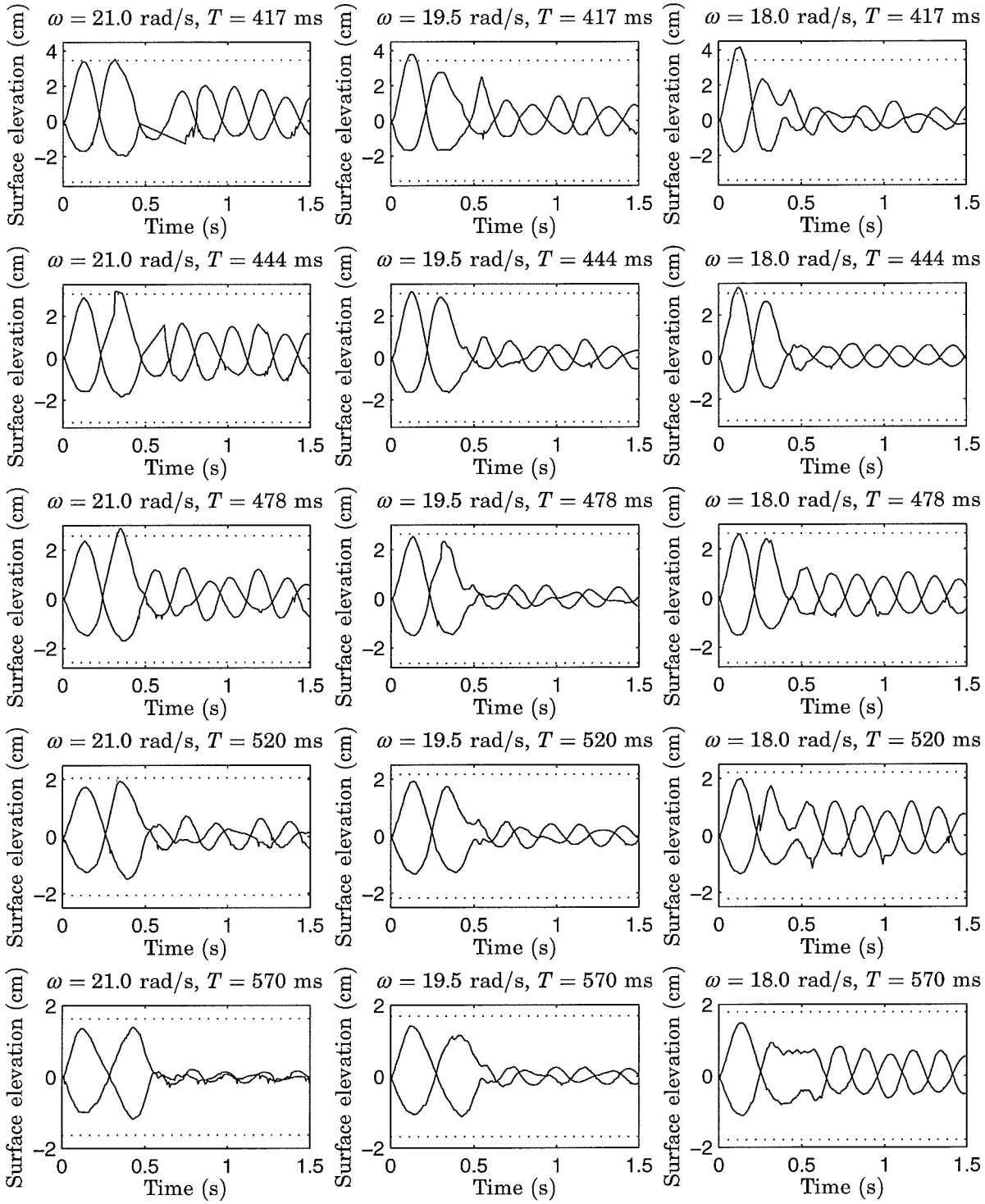

Figure 4.16 Data from experiments with the minimum-energy acceleration profile for movement in several steps for varying values of the movement time T and the oscillation frequency ω in the slosh model used for optimization. The dotted lines show the simulated maximum and minimum slosh, see Table 4.5. Each plot show two experiments, one with the sensor in the front and one with the sensor in the back of the container.

4.7 Modified minimum-energy problem

Analytical solutions to the minimum-energy problem can actually easily be obtained with the following modifications to the constraints:

- The constraint on the control signal (Constraint 1) is removed
- The slosh inequality constraint (Constraint 2) is replaced with a quadratic penalty on the slosh
- The terminal state inequality constraint (Constraint 4b) is replaced with a quadratic penalty on the terminal state

A motivation for the modifications can be found in the numerical solutions of the original minimum-energy problem shown in Figure 4.14 and Figure 4.15. There it can be seen that for the case when $u_{max} = g$ neither the control nor the slosh constraint is active when $\Delta \geq 0.1T_{opt}$.

For the movement in several steps we get the following cost function and constraints

$$\begin{aligned} J &= \frac{1}{2}\int_0^T x^T(t)Qx(t) + Ru^2(t)\ dt \\ x(0) &= [0 \quad 0 \quad 0 \quad 0]^T \\ x(T) &= [0 \quad 0 \quad 0 \quad L]^T \end{aligned} \tag{4.3}$$

and for the movement in one step

$$\begin{aligned} J &= \frac{1}{2}x_{1:2}^T(T)Sx_{1:2}(T) + \frac{1}{2}\int_0^T x^T(t)Qx(t) + Ru^2(t)\ dt \\ x(0) &= [0 \quad 0 \quad 0 \quad 0]^T \\ x_{3:4}(T) &= [0 \quad L]^T \end{aligned} \tag{4.4}$$

The control $u(t)$ that minimizes J is obtained by simultaneously solving the system equation (3.18) and the Euler-Lagrange equations, see Bryson and Ho (1975)

$$\dot{\lambda}^T = -\frac{\partial H}{\partial x} \tag{4.5}$$

$$\frac{\partial H}{\partial u} = 0 \tag{4.6}$$

the Hamiltonian is in both cases

$$H = \frac{1}{2}(x^T Q x + R u^2) + \lambda^T (Ax + Bu)$$

Equations (3.18), (4.5) and (4.6) give

$$\begin{bmatrix} \dot{x} \\ \dot{\lambda} \end{bmatrix} = \underbrace{\begin{bmatrix} A & -\frac{1}{R} B B^T \\ -Q & -A^T \end{bmatrix}}_{M} \begin{bmatrix} x \\ \lambda \end{bmatrix} \tag{4.7}$$

and

$$u = -\frac{1}{R} B^T \lambda \tag{4.8}$$

The solutions to (4.7) can be written as

$$\begin{bmatrix} x(t) \\ \lambda(t) \end{bmatrix} = \Phi(t) \begin{bmatrix} x(0) \\ \lambda(0) \end{bmatrix} \tag{4.9}$$

where $\Phi(t) = e^{Mt}$.

For the movement in several steps we have the boundary values given in (4.3), while $\lambda(0)$ and $\lambda(T)$ are free. Insertion of $x(0)$ in (4.9) then gives

$$x(t) = \Phi_{1:4,5:8}(t)\lambda(0) \tag{4.10}$$

$$\lambda(t) = \Phi_{5:8,5:8}(t)\lambda(0) \tag{4.11}$$

where $\Phi_{1:4,5:8}$ means the sub matrix with row 1 to 4 and column 5 to 8 of $\Phi(t)$. Evaluation of (4.10) at time T gives

$$\lambda(0) = [\Phi_{1:4,5:8}(T)]^{-1} x(T) \tag{4.12}$$

The optimal control $u(t)$ is hence

$$u(t) = -\frac{1}{R} B^T \Phi_{5:8,5:8}(t) [\Phi_{1:4,5:8}(T)]^{-1} x(T) \tag{4.13}$$

For the movement in one step we instead have the boundary values given in (4.4), while $x_{1:2}(T)$ and $\lambda_{3:4}(T)$ are free and

$$\lambda_{1:2}(T) = Sx_{1:2}(T) \tag{4.14}$$

Evaluation of (4.10) at $t = T$ gives

$$x_{3:4}(T) = \Phi_{3:4,5:8}(T)\lambda(0) \tag{4.15}$$

Furthermore, applying (4.10) and (4.11) to (4.14) gives

$$0 = [S\Phi_{1:2,5:8}(T) - \Phi_{5:6,5:8}(T)]\lambda(0) \tag{4.16}$$

Now we can solve for $\lambda(0)$ using (4.15) and (4.16) to obtain

$$\lambda(0) = \begin{bmatrix} S\Phi_{1:2,5:8}(T) - \Phi_{5:6,5:8}(T) \\ \Phi_{3:4,5:8}(T) \end{bmatrix}^{-1} \begin{bmatrix} 0 \\ x_{3:4}(T) \end{bmatrix} \tag{4.17}$$

The optimal control $u(t)$ can be calculated from (4.8), (4.11) and (4.17) and is given by

$$u(t) = -\frac{1}{R}B^T\Phi_{5:8,5:8}(t) \times \begin{bmatrix} S\Phi_{1:2,5:8}(T) - \Phi_{5:6,5:8}(T) \\ \Phi_{3:4,5:8}(T) \end{bmatrix}^{-1} \begin{bmatrix} 0 \\ x_{3:4}(T) \end{bmatrix} \tag{4.18}$$

A special case

In the original minimum-energy problem there is no penalty on the state trajectory, and if the movement time is sufficiently large neither the control nor the slosh constraint is active. This motivates an investigation of the special case when there is no penalty on the state trajectory (i.e. $Q = 0$). When $Q = 0$ and $R = 1$ we get

$$\Phi(t) = \begin{bmatrix} e^{At} & \Phi_{1:4,5:8}(t) \\ 0 & e^{-A^T t} \end{bmatrix}$$

Model with no damping If the damping is neglected in the model (i.e. $\zeta = 0$) we get

$$B^T\Phi_{5:8,5:8}(t) = \begin{bmatrix} \frac{a\omega}{2g}\cos\omega t & -\frac{a\omega}{2g}\sin\omega t & 1 & -t \end{bmatrix}$$

hence for both movement strategies we get

$$u(t) = -\frac{a\omega}{2g}(\lambda_1(0)\cos\omega t - \lambda_2(0)\sin\omega t) - \lambda_3(0) + \lambda_4(0)t \qquad (4.19)$$

where $\lambda(0)$ is given by (4.12) or (4.17) respectively.

Model with damping With the damping in the model (i.e. $\zeta \neq 0$) we get

$$B^T\Phi_{5:8,5:8}(t) = \begin{bmatrix} \frac{a\omega e^{\omega\zeta t}}{2g\sqrt{1-\zeta^2}}(\sqrt{1-\zeta^2}\cos\omega_m t + \zeta\sin\omega_m t) \\ -\frac{a\omega e^{\omega\zeta t}}{2g\sqrt{1-\zeta^2}}\sin\omega_m t \\ 1 \\ -t \end{bmatrix}^T$$

where $\omega_m = \omega\sqrt{1-\zeta^2}$. This gives

$$u(t) = -\frac{a\omega e^{\omega\zeta t}}{2g\sqrt{1-\zeta^2}}[\lambda_1(0)\sqrt{1-\zeta^2}\cos\omega_m t + (\lambda_1(0)\zeta - \lambda_2(0))\sin\omega_m t] - \lambda_3(0) + \lambda_4(0)t \qquad (4.20)$$

for both movement strategies, where $\lambda(0)$ is given by (4.12) or (4.17) respectively.

Experimental evaluation

The control strategies in (4.19) and (4.20) are evaluated for the movement in several steps. The container is moved 0.2 m five times and the movement time is 460 ms and the filling time between the movements is 440 ms.

If we use the nominal value of $\omega = 21.0$ given by (3.13) when calculating the acceleration profile we do not get the expected performance, due to the amplitude dependent oscillation frequency. A way of defining performance for the movement in several steps is to study the remaining oscillation after one movement has been performed.

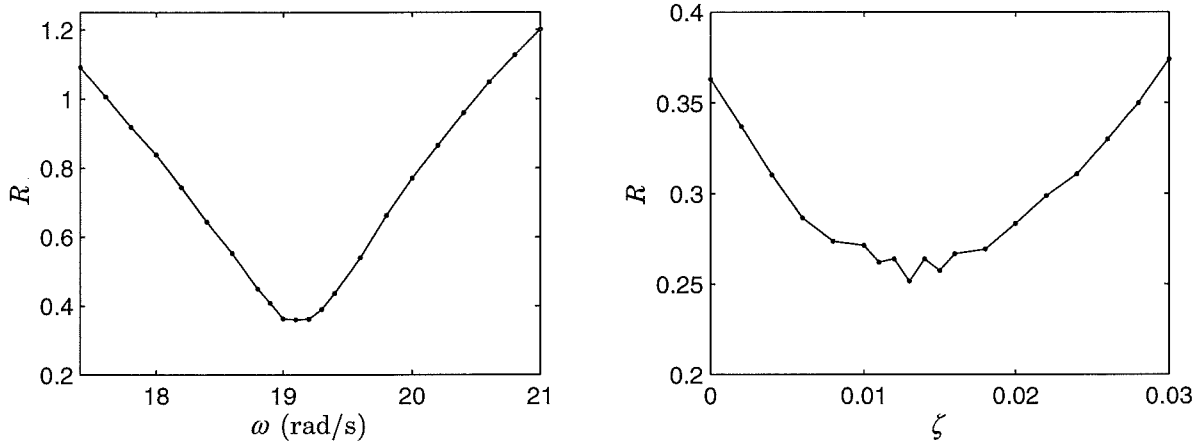

Figure 4.17 The left plot show the performance measure R for different values of ω with $\zeta = 0$, where $\omega = 19.1$ minimizes R. In the right plot R is shown for different values of ζ with $\omega = 19.1$, where $\zeta = 0.013$ minimizes R.

DEFINITION 4.1
Define the residual slosh $r(t)$ as

$$r(t) = s(t + T) \ , \ \text{for } t \geq 0$$

where $s(t)$ is the surface elevation and T is the movement time. The performance measure is then defined as

$$R = \sqrt{\int_0^\infty r^2(t)\, dt}$$

□

To increase the performance, the model parameters ω and ζ were tuned using experiments. First experiments were done with acceleration profiles calculated for different values of ω, with $\zeta = 0$. The performance measure R from these experiments are shown in Figure 4.17. This gave $\omega = 19.1$ as a minimizer of R. This value of ω was then used in the experiments with acceleration profiles calculated for different values of ζ. Figure 4.17 shows R for different values of ζ. The performance measure R is minimized for $\zeta = 0.013$.

In Figure 4.18 the residual slosh is shown for some values of ω. The decrease of the residual slosh amplitude can be seen very clearly

in the figure. However, for $\omega = 19.1$ there is still some residual slosh. Figure 4.19 shows the residual slosh for some values of ζ. The figure shows only a minor decrease of the residual slosh amplitude. The main difference between the experiments done for different values of ζ is the slosh amplitude from $t = 4$ s and forward, where a slight decrease in slosh amplitude can be seen. The oscillation before $t = 4$ s is quite irregular and seems to be a sum of several oscillations with different oscillation frequencies. Ocular inspection shows that the main residual oscillation consists of waves traveling in the direction perpendicular to the movement direction.

The surface elevation when five consecutive movements are performed is shown in Figure 4.20. In Figure 4.21 the surface elevation from each movement cycle is plotted upon each other. The figure shows that there is only a small difference between each movement cycle, and the acceleration profile fulfills the specifications. Since the residual slosh is small the performance is independent of the time between the movements (i.e. the filling time), and therefore the same acceleration profile can be used even if the filling time is changed.

4.8 Conclusions

Several different acceleration strategies have been developed and evaluated. The strategies have been developed using a model of the slosh phenomenon and optimal control techniques. Evaluation of the strategies have been performed in an experimental setup where the surface elevation in the package can be measured.

The minimum-time strategies proved to work only for small values of the maximum surface elevation. Therefore these strategies are only useful if we have a package with a small amount of overhead space or a drive system that only can produce a small maximum acceleration.

With the minimum-energy strategy it is possible to calculate acceleration profiles that work even if the surface oscillation amplitude is large. It is also possible to solve this problem analytically under certain conditions.

In Åström and Furuta (1996) minimum-time and minimum-energy strategies are used to swing up an inverted pendulum. Comparisons show that the minimum-energy strategies are more robust.

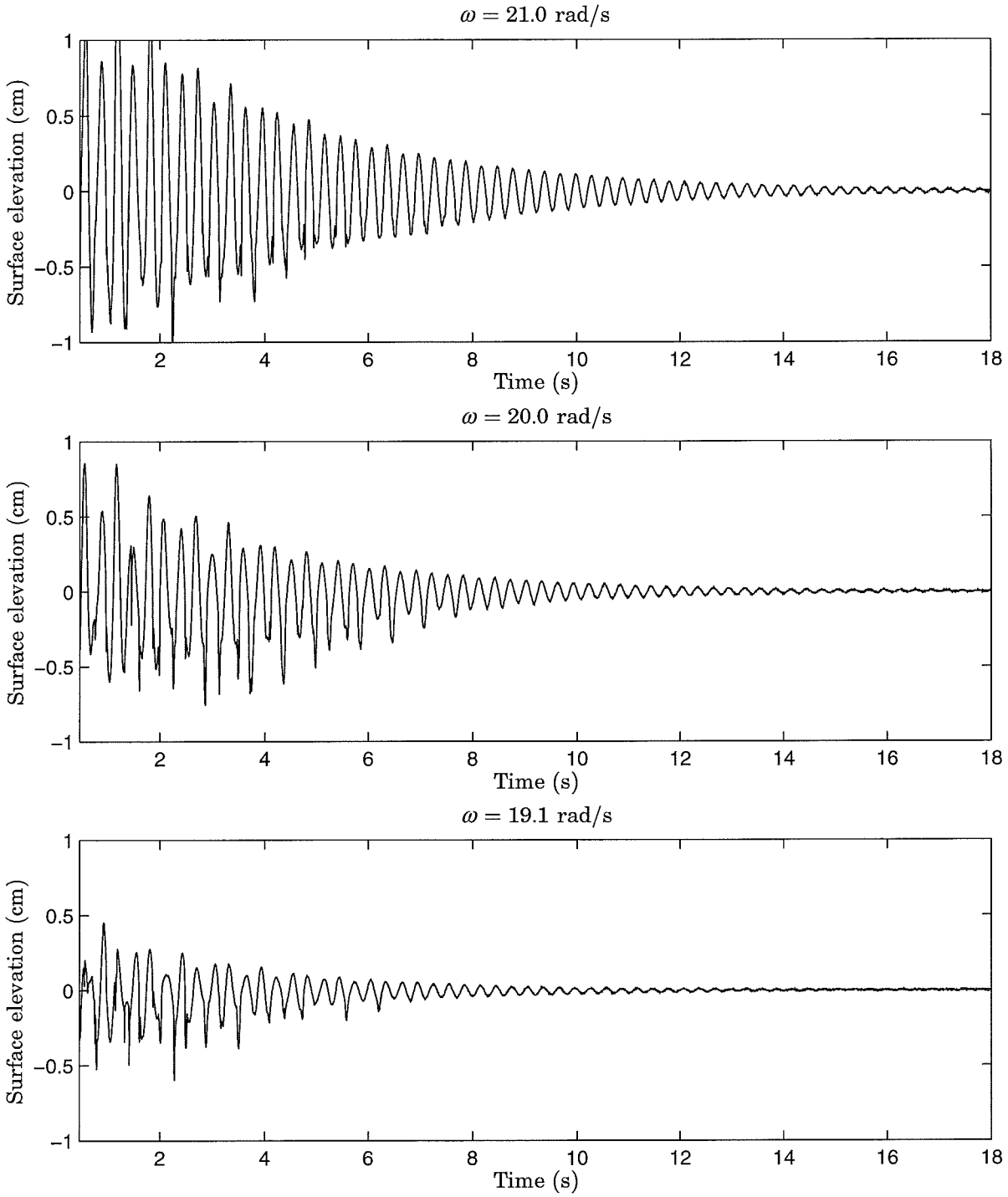

Figure 4.18 Residual slosh for acceleration profiles calculated for different values of ω, with $\zeta = 0$. Best performance is obtained with $\omega = 19.1$ rad/s.

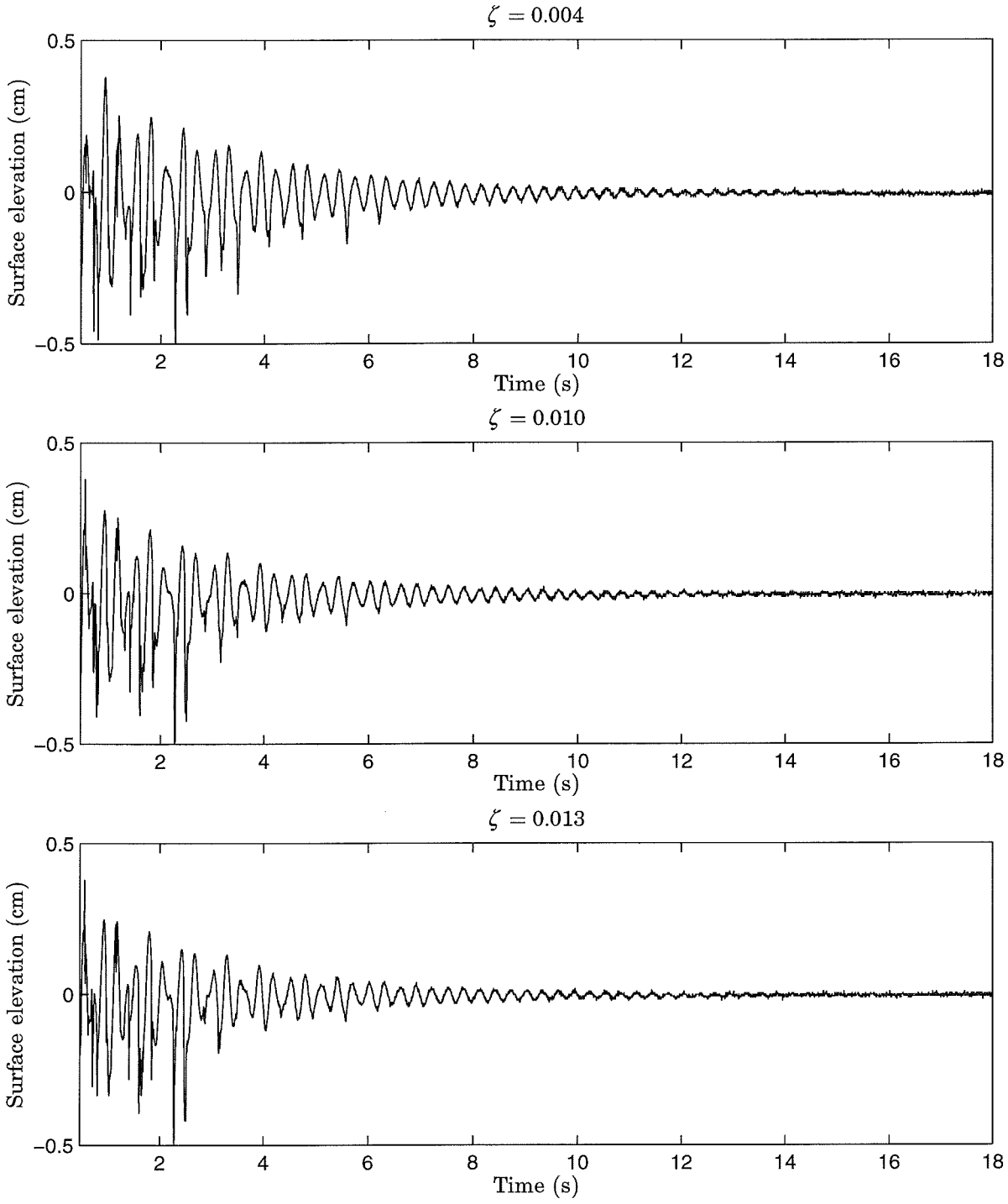

Figure 4.19 Residual slosh for acceleration profiles calculated for different values of ζ, with $\omega = 19.1$.

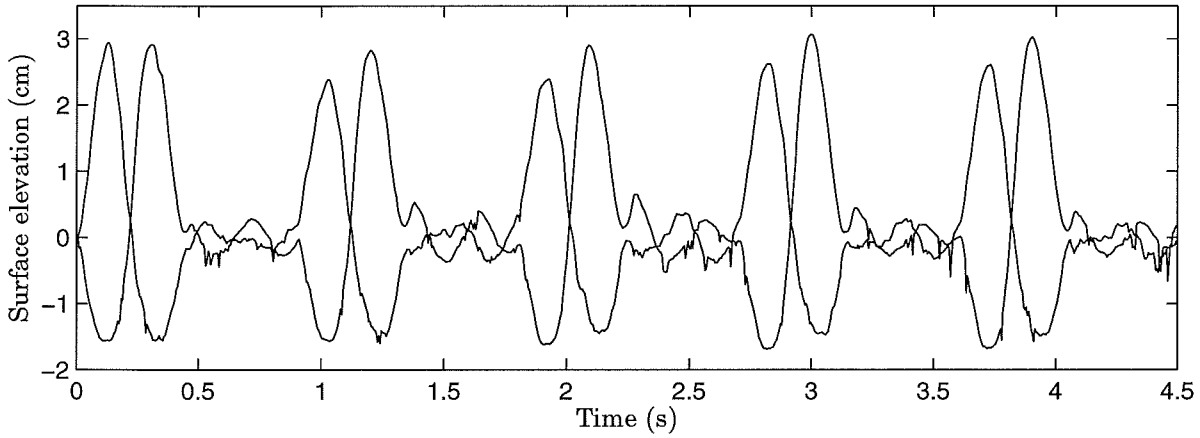

Figure 4.20 Experiment when the container is moved five times showing the surface elevation in the back and in the front. The movement length of each step is $L = 0.2$ m, the movement time is $T = 440$ ms and the time between each step is 460 ms. The performance is satisfactory and the maximum slosh constraint is not violated.

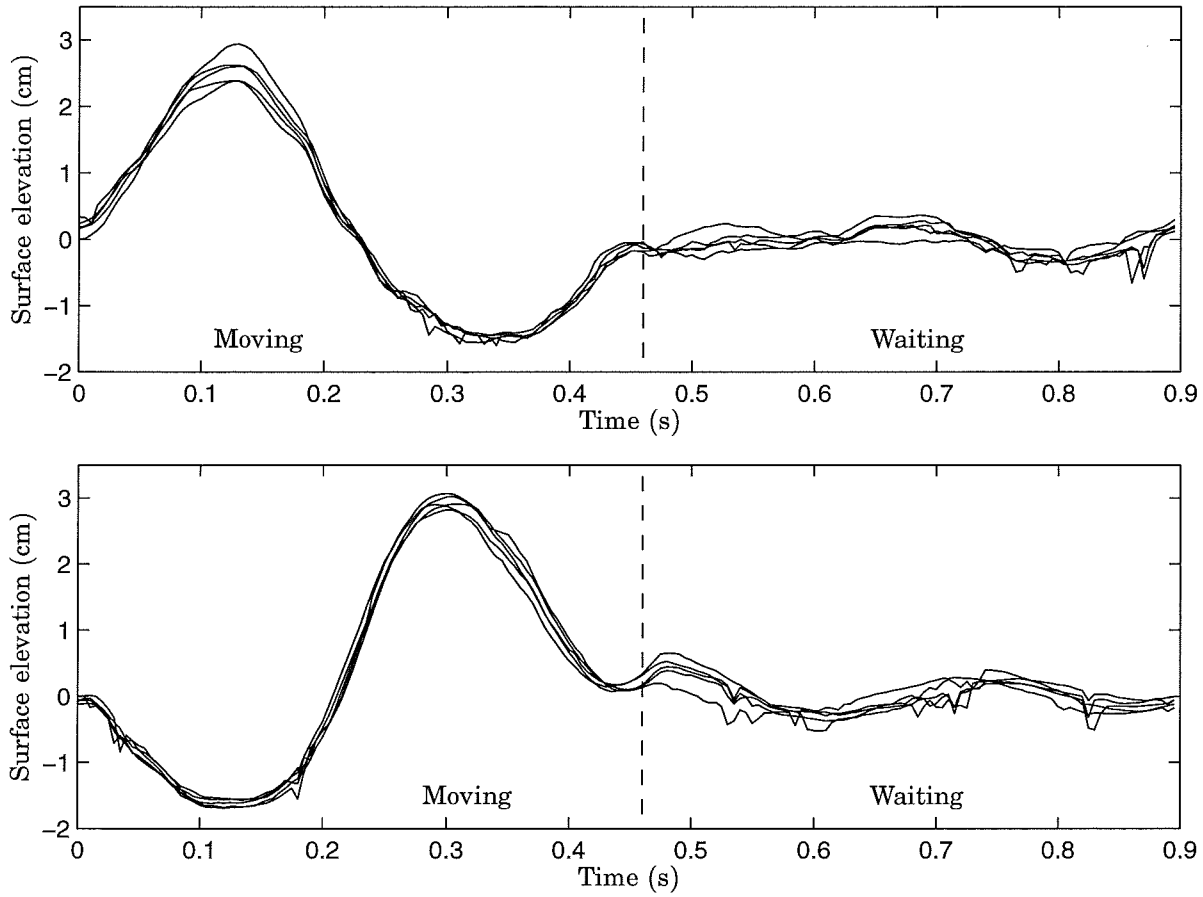

Figure 4.21 Experiment when the container is moved five times showing the surface elevation. The movement cycles are plotted upon each other. To the left of the dashed line the container is moving and to the right of the dashed line it is standing still. The upper plot shows the surface elevation in the back and the lower plot shows the surface elevation in the front.

5

Conclusions and future work

In this thesis an industrially relevant problem has been described where an open container with liquid should be moved quickly without excessive slosh. The major constraint in this problem is to keep the slosh below a certain level during the movement. The problem has been solved first deriving a mathematical model of the slosh phenomenon and then applying optimal control techniques to calculate the appropriate acceleration profile.

The slosh phenomenon has been investigated in experiments and two nonlinear phenomena have been encountered: amplitude dependent oscillation frequency and asymmetric oscillation. A simple second order linear oscillator has been used to model the slosh. Experiments have shown that this model captures the basic behavior of the slosh phenomenon.

Acceleration profiles have been calculated both numerically and analytically by solving different optimal control problems. Two different optimal control problems have been considered: Minimum-time and minimum-energy. These have been solved subject to different constraints, which resulted in four methods for calculating the acceleration profile:

1. *Minimum-time with constraints on maximum acceleration and maximum slosh.*

   This problem is solved numerically and results in a switching ac-

celeration profile that switches between four values. Analytical expressions are given for the switching times in one case. Experiments show that this strategy only works if the maximum slosh is much smaller than the allowed slosh. When the maximum slosh is small, the movement time becomes too large. The reason that the strategy don not work is that a large amount of energy is pumped in and out of the system and that he model does not describe the slosh with sufficient accuracy.

2. *Minimum-time with constraints on maximum acceleration, maximum slosh and maximum stored internal slosh.*

   This problem is solved numerically and results in a switching acceleration profile that switches between four values. Analytical expressions are given for the switching times in one case. This strategy limits the maximum amount of energy stored in the slosh by imposing a maximum constraint on the stored internal slosh. This constraint increases the minimum movement time with 2–4 percent. Experiments show that this strategy works for slightly larger maximum slosh than the original minimum-time strategy. However, the maximum slosh when this strategy works is still much smaller than the maximum allowed slosh.

3. *Minimum-energy with constraints on maximum acceleration and maximum slosh.*

   This problem is solved numerically and results in a smooth acceleration profile. The acceleration profile is calculated by solving a minimum-energy optimal control problem over a fixed time $T = T_{opt} + \Delta$, where T_{opt} is the movement time form the solution of the minimum-time problem and Δ is the extra time we allow for the movement. If Δ is chosen sufficiently large, typically 10–15 percent of T_{opt}, we can obtain acceleration profiles that work well in experiments with shorter movement times than those that are possible to achieve with the minimum-time strategies. The maximum slosh with this strategy is also close to the maximum allowed real slosh. In order to achieve the best performance two parameters in the model need to be adjusted.

4. *Minimum-energy with quadratic penalty on the slosh.*

This problem is solved analytically. If Δ is sufficiently large neither the maximum acceleration nor the maximum slosh constraint is active. This motivates us solve the minimum-energy problem without these constraints.When these constraints are removed the minimum-energy problem is easy to solve analytically.

The main conclusions that can be drawn from the experiments with the different acceleration strategies are that:

- the minimum-time strategies are sensitive to model discrepancies
- the minimum-time strategies can only be used if the maximum allowed slosh is small
- the minimum-energy strategy does not excite the unmodelled dynamics of the slosh
- the minimum-energy strategy can be used when the maximum allowed slosh is large
- the minimum-energy problem can be solved analytically under certain conditions and gives simple expressions for the acceleration profile

There are many possible future extensions of this work both theoretically and practically.

The main theoretical extension is to refine the slosh model so that it captures some of the most important nonlinear phenomena encountered in the experiments. With a more elaborate model it might be possible to calculate the acceleration profile without adjusting the model parameters. It is also possible that the solution of the minimum-time problem with a better model works even for large maximum slosh.

On the practical side it would be interesting to try the developed strategies on different package geometries, different fluids and when the movement is rotational instead of linear. It is also of interest to design simple experiments that can identify how the model parameters should be adjusted to get the best performance when the minimum-energy strategy is used.

6

Bibliography

ARMENIO, V. (1992): *Dynamic behavior of free surface liquids on ships.* PhD thesis, Department of Naval Architecture, Ocean and Environmental Engineering, University of Trieste, Trieste, Italy.

ARMENIO, V. and M. LA ROCCA (1996): "On the analysis of sloshing of water in rectangular containers: Numerical study and experimental validation." *Ocean Engineering*, **23:8**, pp. 705–739.

ÅSTRÖM, K. J. and K. FURUTA (1996): "Swinging up a pendulum by energy control." In *IFAC'96, Preprints 13th World Congress of IFAC*, vol. E, pp. 37–42. San Francisco, California.

BALDOCK, G. R. and T. BRIDGEMAN (1981): *The Mathematical Theory of Wave Motion.* Ellis Horwood Limited.

BRYSON, A. E. (1994): *Control of Spacecraft and Aircraft.* Princeton University Press.

BRYSON, A. E. and Y. HO (1975): *Applied Optimal Control: Optimization, Estimation and Control.* Hemisphere Publishing Corporation, New York. Revised Printing.

COULSON, C. A. (1955): *Waves*, 7 edition. University Mathematical Texts. Interscience Publishers.

CRAWLEY, E. F., R. J. HANSEN, and L. D. PETERSON (1989): "Nonlinear fluid slosh coupled to the dynamics of a spacecraft." *AIAA Journal*, **27:9**, pp. 1230–1240.

DIETZE, S. and F. J. SCHMIDT (1997): "Entwurf zur optimalsteuerung offener behälter zum förden von fluiden in verarbeitungsmaschinen." Technical Report MATH-NM-13-1997. Technische Universität Dresden, Dreseden, Germany.

DUBOIS, F., N. PETIT, and P. ROUCHON (1998): "Motion planning and nonlinear simulations for a tank containing a fluid." Technical Report 494. Centre Automatique et Systèmes, Ecole Nationale Supérieure des Mines de Paris, Paris, France.

FEDDEMA, J. T., C. R. DOHRMANN, G. G. PARKER, R. D. ROBINETT, V. J. ROMERO, and D. J. SCHMITT (1997): "Control for slosh-free motion of an open container." *IEEE Control Systems*, **17:1**, pp. 29–36.

GRAHAM, E. W. and A. M. RODRIGUEZ (1952): "Characteristics of fuel motion which affect airplane dynamics." *Journal of Applied Mechanics*, **19**, pp. 381–388.

GUSTAFSSON, T. (1995): "Modelling and control of a rotary crane." In *Proceedings of the 3rd European Control Conference*. Rome, Italy.

KELKAR, K. M. and S. V. PATANKAR (1997): "Numerical method for the prediction of free surface flows in domains with moving boundaries." *Numerical Heat Transfer, Part B: Fundamentals*, **31:1**, pp. 387–399.

LAMB, H. (1945): *Hydrodynamics*, 6 edition. Dover Publications.

LEE, H., S. CHO, and J. CHO (1997): "A new anti-swing control of overhead cranes." In *Proceedings of the IFAC International Workshop on Automation in the Steel Industry*. Kyongju, Korea.

MÅRTENSSON, K. (1972): *New Approaches to the Numerical Solution of Optimal Control Problems*. PhD thesis, Department of Automatic Control, Lund Institute of Technology, Lund, Sweden.

ROMERO, V. J. and M. S. INGBER (1995): "A numerical model for 2-D sloshing of pseudo-viscous liquids in horizontally accelerated rectangular containers." In BREBBIA *et al.*, Eds., *Boundary Elements XVII*, pp. 567–583. Computational Mechanics Publications, Southampton, England.

SANKAR, S., R. RANGANATHAN, and S. RAKHEYA (1992): "Impact of dynamic fluid slosh loads on the directional response of tank vehicles." *Vehicle System Dynamics*, **21:6**, pp. 385–404.

SCHWARTZ, A. L. and E. POLAK (1996): *RIOTS: A Matlab Toolbox for Solving Optimal Control Problems Version 1.0.* University of California Berkeley, Berkeley, California.

SHEN, S. S. (1993): *A Course on Nonlinear Waves.* Kluwer Academic Publishers.

VENUGOPAL, R. and D. S. BERNSTEIN (1996): "State space modeling and active control of slosh." In *Proceedings of the 1996 IEEE International Conference on Control Applications*, pp. 1072–1077. Dearborn, Michigan.